Journal Pre-proof

Mass accumulation rates decreased in the Skagerrak basin over the last 100 years

Timo Spiegel, Andrew W. Dale, Nina Lenz, Mark Schmidt, Matthias Moros, Sebastian Lindhorst, Hendrik Wolschke, Daniel Müller, Martin Butzin, Michael Fuhr, Habeeb Thanveer Kalapurakkal, Sabine Kasten, Klaus Wallmann

PII: S0278-4343(25)00011-1

DOI: https://doi.org/10.1016/j.csr.2025.105411

Reference: CSR 105411

To appear in: *Continental Shelf Research*

Received Date: 2 August 2024

Revised Date: 13 January 2025

Accepted Date: 20 January 2025

Please cite this article as: Spiegel, T., Dale, A.W., Lenz, N., Schmidt, M., Moros, M., Lindhorst, S., Wolschke, H., Müller, D., Butzin, M., Fuhr, M., Kalapurakkal, H.T., Kasten, S., Wallmann, K., Mass accumulation rates decreased in the Skagerrak basin over the last 100 years, *Continental Shelf Research*, https://doi.org/10.1016/j.csr.2025.105411.

Mass accumulation rates decreased in the Skagerrak basin over the last 100 years

Timo Spiegel[1,2*], Andrew W. Dale[1], Nina Lenz[1], Mark Schmidt[1], Matthias Moros[3], Sebastian Lindhorst[2], Hendrik Wolschke[4], Daniel Müller[5,6], Martin Butzin[7], Michael Fuhr[1], Habeeb Thanveer Kalapurakkal[1], Sabine Kasten[5,6,7], Klaus Wallmann[1]

[1] GEOMAR Helmholtz Centre for Ocean Research Kiel, Wischhofstraße 1–3, 24148 Kiel, Germany

[2] Universität Hamburg, Institut für Geologie, Bundesstr. 55, 20146 Hamburg, Germany

[3] Leibniz Institute for Baltic Sea Research Warnemünde, Seestraße 15, DE-18119 Rostock, Germany

[4] Helmholtz-Zentrum Hereon, Institute of Coastal Environmental Chemistry, Max-Planck Str. 1, 21502, Geesthacht, Germany

[5] Alfred Wegener Institute Helmholtz Centre for Polar and Marine Research, Am Handelshafen 12, 27570 Bremerhaven, Germany

[6] University of Bremen, Faculty of Geosciences, Klagenfurter Straße 4, 28359 Bremen, Germany

[7] MARUM - Center for Marine Environmental Sciences University of Bremen, Leobener Straße 8 28359 Bremen, Germany

***Correspondence:**
Timo Spiegel
tspiegel@geomar.de

Keywords: Temporal variability, Age-depth model, Bioturbation, North Sea, ^{210}Pb, ^{137}Cs, ^{14}C.

Abstract

Since the 19th century, the North Sea sediment system has been subject to a dynamic hydrographic regime and intense human alteration. The Skagerrak serves as the largest depocenter for suspended sediment originating from the North Sea. Thus, deposits in the Skagerrak provide a historical record of potential shifts in the sediment cycle of the North Sea. Despite the availability of mass accumulation rate (MAR) data in the Skagerrak, previous studies focused on steady-state reconstructions and little is known about how these rates may have changed over time. To address this knowledge gap, we present age-depth models based on the natural radionuclide ^{210}Pb and the anthropogenic time markers ^{137}Cs, fraction modern ^{14}C (F^{14}C) and mercury (Hg) to determine the MAR before and after the year 1963 at six stations in the deep Skagerrak basin between 434 and 677 meters water depth. We applied 1963 as the boundary since this year is constrained by ^{137}Cs and F^{14}C peaks in the sediment cores due to atomic weapons testing and changes in sedimentary Hg contents.

Our primary result reveals that the MAR in the deep Skagerrak basin decreased from 0.17 to 0.14 g cm^{-2} yr^{-1} averaged across the stations. We further simulate the effect of bioturbation on the solid phase profiles by applying a reaction transport model to the data, revealing that the decline in MAR is more pronounced when bioturbation is considered (from 0.17 to 0.09 g cm^{-2} yr^{-1}). Decreasing MARs in the Skagerrak basin indicate that the sediment system of the North Sea substantially changed over time. Possible reasons include a shift in the North Sea circulation pattern, enhanced sediment trapping in the Wadden Sea and reduced sediment inputs due to river damming, deepening of harbor channels and coastal protection. However, we stress that our data do not allow for a quantitative analysis of the major driving factors behind the temporal variability of sediment cycling. Hence, we recommend combining our results with information on the provenance of the Skagerrak deposits and integrating the Skagerrak data into larger-scale physical models that consider non-steady state particle transport in the North Sea.

1. Introduction

The sediment dynamics of the North Sea region are driven by several factors, including circulation patterns, waves, tides, storms, riverine discharge, and coastal erosion (Stride, 1982; Eisma and Irion, 1988; Green et al., 1995; Elliott et al., 1998; Holland and Elmore, 2008; Stanev et al., 2009; Fettweis et al., 2010; Dangendorf et al., 2014). However, the sediment cycle is regulated not just by natural processes but also by multiple human activities including bottom trawling (Eigaard et al., 2017; ICES, 2020; Rijnsdorp et al., 2020), dredging and sediment extraction (De Groot, 1986; ICES, 2019; Mielck et al., 2019), the construction of offshore wind farms (Baeye and Fettweis, 2015; Slavik et al., 2019; Daewel et al., 2022; Heinatz and Scheffold, 2023), coastal protection and land reclamation (Kelletat, 1992; Hoeksema, 2007; Hofstede, 2008), river damming (IKSE, 2005; Lange et al., 2008; IKSE, 2012; Hübner and Schwandt, 2018) and eutrophication (Pätsch et al., 2010; Skogen et al., 2014; Axe et al., 2017). Since 1900, these human activities and their environmental impact notably increased in the North Sea region (ICES, 2018, 2019, 2020; OSPAR, 2023). Hence, the sediment system of the North Sea may have undergone changes over time due to natural and human processes, considering the economic pressure, the region's dynamic environment and the impact of climate change.

The sediment cycle governs the cycling of elements and compounds in the ocean, such as organic carbon (OC), nutrients and pollutants. Hence, both human and natural impacts may also affect the biogeochemistry of the North Sea. For instance, disturbance of the seafloor reintroduces sedimentary OC into the oxygenated water column, which can enhance OC respiration rates and modify the atmospheric CO_2 uptake by the ocean. The degree of sedimentary OC loss due to bottom trawling (Bradshaw et al., 2021; Sala et al., 2021; Hiddink et al., 2023) and the balance between OC loss and OC trapping in wind park areas (Heinatz and Scheffold, 2023) are currently debated. Hence, it is crucial to assess how the sedimentary system of the North Sea may have changed over time to safeguard its ecological value and establish a baseline for resource management plans.

Approximately 45 - 80 % of the total suspended sediment input to the North Sea accumulates in the Skagerrak (Oost et al., 2021; Spiegel et al., 2024a). Hence, the sedimentary archives of the Skagerrak mirror the sediment system of the entire North Sea region under changing environmental conditions. Despite the large amount of available sedimentary records for the Skagerrak (Erlenkeuser and Pederstad, 1984; Bjørnstad et al., 1985; Erlenkeuser, 1985; van Weering et al., 1987, 1993; Paetzel et al., 1994; Alve, 1996; Bøe et al., 1996; Ståhl et al., 2004; Deng et al., 2020), little is known about the temporal variability of sediment transport into the Skagerrak. In this study, we investigate how mass accumulation rates (MAR) at six stations in the deep Skagerrak basin have changed over time based on age-depth modeling. Therefore, we determined mean MARs in surface sediments deposited since 1963 and mean MAR in subsurface sediments deposited prior to 1963 using anthropogenic time markers and the natural radionuclide ^{210}Pb, respectively. In the upper part of the sediment cores, age-depth relationships were obtained from data on caesium-137 (^{137}Cs), fraction modern carbon-14 (F^{14}C) and mercury (Hg), which serve as time markers of the year 1963. The activity peaks of ^{137}Cs and F^{14}C reflect the atmospheric nuclear weapon tests that were most prevalent in 1963 (van Weering et al., 1993; Deng et al., 2020), while the peaks in Hg concentrations result from its economic utilization prior to regulations between 1960 and 1970 (Leipe et al., 2013; Moros et al., 2017; Polovodova Asteman et al., 2018). However, benthic organisms can alter the time marker signals by feeding, burrowing and particle mixing in marine sediments, a process which is summarized as bioturbation (Richter, 1952; Rhoads, 1974; Aller, 1982; Meysman et al., 2006). In order to understand the effect of bioturbation on the MAR in the upper sediment section, we present a reaction transport model that simultaneously calculates the burial of solids and sediment mixing by bioturbation. Below the time marker depths, the constant flux constant sedimentation (CFCS) model is applied to excess lead-210 ($^{210}Pb_{ex}$) data (Krishnaswamy et al., 1971; Sanchez-Cabeza and Ruiz-Fernández, 2012) to derive age-depth relationships. This approach of virtually splitting the sediment core into two sections allows for the determination of average MARs before and after the year 1963 to present a general temporal trend for sediment deposition in the Skagerrak basin. Subsequently, we discuss the MAR temporal variability within the Skagerrak basin in relation to potential driving forces that could have altered the sediment system of the North Sea.

2. Study area

The Skagerrak strait is located between Denmark, Norway and Sweden and links the North Sea and the Kattegat with a maximum water depth of approximately 700 meters (Fig. 1a). Surface waters in the Skagerrak circulate anticlockwise. Water from the North Sea enters the Skagerrak through the Tampen Bank Current and the Central North Sea Current from the north and west and through the Jutland Current from the south, which, together with the Baltic Current, results in the outflowing Norwegian Coastal Current leaving the Skagerrak to the north (Rodhe, 1987, 1996; van Weering et al., 1987; Otto et al., 1990). Annual total sediment deposition in the Skagerrak amounts to about 35 Mt yr^{-1} (Spiegel et al., 2024a). Skagerrak sediments are characterized by a large lateral input of mostly lithogenic material from the North Sea (van Weering et al., 1993; De Haas and van Weering, 1997; Spiegel et al., 2023, 2024a). The sediment composition comprises fine-grained silt and clay sediments in the deeper parts of the Skagerrak, where current velocities decrease and the fine material can settle. In contrast, sandy deposits (<40% clay) reflect sediment erosion and transportation along the more energetic Danish coastlines (Bergsten et al., 1996; Stevens et al., 1996). On a larger scale, the Skagerrak is connected to the currents in the North Sea (Fig. 1b). Water that is transported into the North Sea through the northern Atlantic entrance is split into two currents. The first one, the Dooley Current, flows eastwards and supplies the Central North Sea Current, which carries the water further into the Skagerrak. Furthermore, the Dooley Current combines with the water inflow from the Tampen Bank area forming a deep water current at 200 - 400 meters water depth at the southern Norwegian Trench transporting water into the Skagerrak (Rodhe, 1996). This current likely represents a major source of the suspended matter that settles in the deep Skagerrak basin (Rodhe and Holt, 1996). The second current, the Scottish Coastal Current, moves southwards until it converges with the inflow of Atlantic water from the English Channel in the southern North

Sea. The resulting water mass is transported northwards via the Jutland Current to the Skagerrak (Otto et al., 1990; Rodhe, 1998; Winther and Johannessen, 2006).

3. Material and methods

3.1 Sampling

We present data from six stations (434 to 677 meters water depth) in the Skagerrak basin. Sampling was performed during two research cruises with R/V Alkor, AL557 in June and AL561 in August 2021, respectively (Schmidt, 2021; Thomas et al., 2022). At each station, a short sediment core was recovered (<50cm) using a multiple-corer (MUC). Sediment samples for porosity and solid phase analysis were taken at every centimeter of the MUCs, whereby the entire material over the core surface area (63.6 cm^2) of each interval was transferred into whirlpacks. The samples were stored refrigerated at 4°C until further home-based processing.

3.2 Analytical techniques

Wet sediment samples were weighted, subsequently freeze-dried and weighed again to determine wet and dry sediment mass. Porosity in the sediment samples was determined from the loss of water after freeze-drying assuming a density of dry solids of 2.5 g cm^{-3}. For the analysis of ^{210}Pb and ^{137}Cs, the freeze-dried sediment was homogenized and subsequently embedded into containers that were sealed with a two-component epoxy resin. Steady-state equilibration between ^{226}Ra and ^{214}Bi was achieved by storing the samples for two weeks. Analysis of total ^{210}Pb and ^{137}Cs activities was carried out by gamma spectrometry on n-type planar or coaxial Ge-detectors at GEOMAR (MUC5), IOW Warnemünde (MUC2, MUC7 and MUC8), Göttingen (St.65) and IAF Dresden (MUC9). The natural background decay of ^{226}Ra (295 keV) in marine sediments was subtracted from the total ^{210}Pb activities to obtain the excess ^{210}Pb ($^{210}Pb_{ex}$) values.

Radiocarbon analyses were performed on benthic infaunal foraminiferal assemblages at stations MUC2, MUC7 and MUC8. Sediment samples were gently washed through a 63 µm sieve and subsequently dried at 40°C. Only well-preserved individuals were collected and subsequently sorted by species. The foraminiferal species used in this study have been described in detail in the literature and included *Bolivina skagerrakensis, Bulimina marginata, Uvigerina mediterranea, Ammonia beccari batavus, Melonis barleeanum and Nonionellina labradorica* (van Weering and Qvale, 1983; Qvale and Nigam, 1985; Nordberg and Bergsten, 1988; Conradsen et al., 1994; Heier-Nielsen et al., 1995; Alve, 1996; Bergsten et al., 1996; Hass, 1996; Gyllencreutz et al., 2006). Radiocarbon analyses were performed using a MICADAS micro-scale AMS following standard procedures as described in Mollenhauer et al. (2021). Samples were processed by acid hydrolysis of foraminifera tests containing between 59 and 96 µg carbon in a CHS system directly connected to the MICADAS via the Gas Interface System (Wacker et al., 2013). Results were reported as fraction modern ($F^{14}C$) expressed relative to the atmospheric ^{14}C content in 1950 (Reimer et al., 2004).

The content of Hg was measured in 20 - 100 mg of dried sediment at every centimeter using a DMA-80 Analyser from MLS Company, following the method described in Leipe et al. (2013). The certified reference material CRM (BCR) 142R and the soil standard SRM 2709 were used for calibration. For further details on the method and data quality, see Leipe et al. (2013).

Bulk sediment grain-size distributions were determined for each station except St.65. A volume of 1.5 cm^3 was sampled equidistantly from each centimeter slice of the sediment cores. Samples were treated with 10% - 30% hydrogen peroxide and 60% acetic acid to dissolve organic and carbonate compounds. Subsequently, samples were dispersed in water using tetra-sodium diphosphate decahydrate. Grain-size distributions were determined at the CEN, University of Hamburg, with a laser-diffraction particle-sizer (Sympatec HELOS/KF Magic; range 0.5/18 to 3500 µm). Accuracy of measurements and absence of a long-term instrumental drift were ensured by regular analysis of an in-house standard (standard deviation for mean grain size and D_{50} over the analysis period was < 1.1 µm). Statistical evaluation of grain-size distributions was based on the graphical method (Folk and Ward, 1957), calculated using Gradistat (Blott and Pye, 2001).

3.3 Age-depth modeling

3.3.1 Modeling approach

In order to derive a general temporal trend of the MAR in the Skagerrak basin, the sediment cores were divided into a surface section and a deep section and the MARs were determined in both sections individually. The boundary between the sections was defined by the activity or concentration peaks of the time marker triplet ^{137}Cs, Hg and $F^{14}C$ that relate a certain sediment depth in each core to the year 1963. The time marker triplet was assumed to represent the year 1963 since ^{137}Cs and $F^{14}C$ were excessively introduced into the atmosphere by nuclear weapon tests in this year (van Weering et al., 1993; Deng et al., 2020) and economic utilization of Hg was regulated between 1960 - 1970 (Leipe et al., 2013; Moros et al., 2017; Polovodova Asteman et al., 2018). The MAR in the upper section was determined by the total accumulated dry sediment mass in the sediment core up to the sediment depth of the time marker peak. In the absence of a further time marker below the 1963 peaks, age-depth relationships in the deeper sediment section were derived based on the continuous decay of $^{210}Pb_{ex}$ in the sediments (Krishnaswamy et al., 1971; Robbins and Edgington, 1975; Appleby and Oldfieldz, 1983). Here, we applied the CFCS model following the workflow presented in Sanchez-Cabeza and Ruiz-Fernández (2012). Given that the dry mass was used to determine the MARs in both sections, our calculations consider the effect of compaction on marine sediments. However, sediment mixing (i.e. bioturbation) in surface sediments is neglected applying this approach. Hence, we further set up a reaction transport model to simulate the potential effects of bioturbation on the time marker profiles in the upper sediments. It is important to note that the methodology employed to derive the MARs from two self-chosen sediment core sections does not reflect the actual timing, magnitude and number of MAR changes that may have occurred in the natural system. Instead, we present a general temporal trend across the stations in the Skagerrak basin by comparing the MARs before and after the year 1963.

3.3.2 Upper sediment section

The MAR in the upper sediment section was calculated as:

$$\mathrm{MAR} = \frac{\sum \mathrm{M}}{\mathrm{S} \cdot (\mathrm{T}_0 - 1963)} \quad (1)$$

where ∑M is the sum of the measured dry sediment masses up to the observed depth of the ^{137}Cs peak, S is the surface area of the MUCs (63.3 cm^2), 1963 corresponds to the year defined by the ^{137}Cs peak and T_0 denotes the time of sample collection (year, in A.D.).

3.3.3 Deep sediment section

The MAR in the sediment section below the depth of the time marker peaks was determined based on the CFCS method following the workflow presented in Sanchez-Cabeza and Ruiz-Fernández (2012). Assuming no post-depositional redistributions and constant ^{210}Pb fluxes to the sediments, the MAR can be derived from linear regression analysis relating the logarithmic $^{210}Pb_{ex}$ activities to mass depths (Fig. 2). The MAR was then calculated as:

$$\mathrm{MAR} = \frac{-\lambda}{\mathrm{m}} \quad (2)$$

where λ is the decay constant of ^{210}Pb (0.03118 yr^{-1}) and m is the slope of the linear regression fit of the logarithmic $^{210}Pb_{ex}$ activity and mass depth plot. Mass depth refers to the sum of dry sediment masses above the sampled depth in the sediment core.

3.3.4 Reaction transport model description

In order to simulate the effect of bioturbation on the MARs, we applied a numerical reaction transport model to the data of the upper sediment section. Such models have been widely used to mathematically describe sedimentation and mixing processes based on downcore $^{210}Pb_{ex}$ and ^{137}Cs distributions (Peng et al., 1979; Boudreau, 1986; Robbins, 1986; Crusius and Kenna, 2007). They typically consist of transport and reaction terms that determine how the concentrations of sedimentary constituents vary over space and time. In this model, the transport processes included the burial of solids affected by sediment compaction and solid phase mixing by bioturbation, which were treated as downward-directed advection and as diffusive transport along concentration gradients, respectively. The decay of the radioisotopes represents the reactions in the model. As such, the down-core distributions of $^{210}Pb_{ex}$, ^{137}Cs, $F^{14}C$ and Hg were calculated with the following one-dimensional partial differential equation:

$$\mathrm{ds}(1-\phi)\frac{\partial \mathrm{C}}{\partial \mathrm{t}} = \frac{\partial}{\partial \mathrm{x}}\left(\mathrm{ds}\,(1-\phi)\,\mathrm{D_B}\frac{\partial \mathrm{C}}{\partial \mathrm{x}} - \mathrm{ds}\,(1-\phi)\,\mathrm{u_s}\,\mathrm{C}\right) - \mathrm{ds}(1-\phi)\,\lambda_\mathrm{C}\,\mathrm{C} \quad (3)$$

where C is the activity or concentration, ds is the density of dry solids (2.5 g cm^{-3}), ϕ is porosity, D_B is the bioturbation coefficient, u_s is the burial velocity and λ_C are the decay constants of ^{137}Cs (0.023 yr^{-1}), $F^{14}C$ (0.00012 yr^{-1}) and Hg (0 yr^{-1}, no decay), respectively. Bioturbation was treated as biodiffusive intraphase mixing in this equation as described in Boudreau (1997). The change of the bioturbation rate with depth was described as:

$$D_B = D_{B0} \cdot \exp\left(-\frac{x^2}{2 \cdot {x_B}^2}\right) \quad (4)$$

where D_{B0} is the bioturbation coefficient at the sediment-water interface and x_B controls the bioturbation mixing depth.

Steady-state sediment compaction was considered in the model by using the following function to fit the porosity data (Berner, 1980):

$$\phi = \phi_c + (\phi_0 - \phi_c)^{(-x \cdot p_x)} \quad (5)$$

where ϕ_0 is the porosity at the sediment surface, ϕ_c is the porosity in compacted sediment and px is the attenuation coefficient. Burial velocities were described as:

$$u_s = \frac{SR \cdot (1 - \phi_c)}{(1 - \phi)} \quad (6)$$

where SR is the sedimentation rate after compaction.

Upper boundary conditions for $^{210}Pb_{ex}$, ^{137}Cs, $F^{14}C$ and Hg were set as temporally variable fluxes to the seafloor:

$$FC(t) = MAR(t) \cdot C_0(t) \quad (7)$$

where FC(t) is the flux to the seafloor and $C_0(t)$ is the activity or concentration in settling particles. In the case of $^{210}Pb_{ex}$, a constant $^{210}Pb_{ex}$ activity in particles settling to the seafloor was assumed following the CIC method (Appleby and Oldfieldz, 1983; Sanchez-Cabeza and Ruiz-Fernández, 2012). Hence, $C_0(t)$ in Eq. 7 was set temporally constant and we refer to it as Pb_0 in the following. The value of Pb_0 is typically determined by extrapolating the $^{210}Pb_{ex}$ data towards the sediment surface using exponential regression (Sanchez-Cabeza and Ruiz-Fernández, 2012). However, sediment mixing was assumed to occur within the upper part of the sediment cores, which can lead to uncertainty in such extrapolations. Hence, Pb_0 was chosen to be a fitting parameter for $^{210}Pb_{ex}$ in the model simulations. For the time markers ^{137}Cs and Hg, $C_0(t)$ was determined using an interpolation function that was fitted to time series data presented in previous studies for atmospheric deposition of ^{137}Cs in the northern hemisphere (Garcia Agudo, 1998) and global Hg emissions into the atmosphere (Hylander and Meili, 2003; Streets et al., 2011). The period of enhanced Hg input corresponding to the extensive American gold mining period between 1860 and 1920 was not considered in our model, as the Hg data in the sediment cores did not reflect this input. For $F^{14}C$, we approximated $C_0(t)$ with dissolved inorganic radiocarbon concentrations of surface water ($F^{14}C_{DIC}$) simulated using the ocean general circulation model FESOM2 (Danilov et al., 2017; for the implementation of $F^{14}C_{DIC}$ see Lohmann et al., 2020; Butzin et al., 2023). The model considered $F^{14}C_{DIC}$ as a single abiotic tracer which was connected with the carbon cycle only through $^{14}CO_2$ air-sea exchange calculated according to Wanninkhof (2014) and assuming a homogeneous concentration of 2000 mmol m^{-3} of DIC in surface water following Toggweiler et al. (1989). FESOM2 was run from 1850 CE to 2015 CE with prescribed periodic climate forcing (Large and Yeager, 2009) as well as with transient values of atmospheric CO_2 (Meinshausen et al., 2017) and $F^{14}C$ (Graven et al., 2017), starting from preindustrial conditions determined in a previous study (Lohmann et al., 2020). Overall, the simulated anthropogenic $F^{14}C_{DIC}$ distribution was in line with global observations (Key et al., 2004; Butzin et al., 2021). FESOM2 employs unstructured meshes with variable horizontal metric resolution. Here, the resolution was about 127,000 surface nodes in the horizontal and 47 layers in the vertical. The model results were remapped to regular geographical coordinates and evaluated nearest to the core sites. The temporal variability of $C_0(t)$ for ^{137}Cs, $F^{14}C$ and Hg that were used to calculate upper boundary fluxes and the calculated upper boundary fluxes for all parameters are shown in the supplement (Fig. S1, S2). At the lower model boundary (50 cm), a zero gradient condition was imposed for all model variables.

In total, seven parameters (MAR, Pb_0, ϕ_0, ϕ_c, px, D_{B0}, x_B) were adjusted to fit the porosity, $^{210}Pb_{ex}$ ^{137}Cs, $F^{14}C$ and Hg data in the upper sediment section. The parameters ϕ_0, ϕ_c and px were determined by visually fitting the measured porosity data (Fig. 3). The MAR, Pb_0, DB_0 and x_B parameters were first evaluated by a Monte Carlo-type approach (3000 runs) after Dale et al. (2021). For each Monte Carlo run, a random configuration of the three parameters was selected within the ranges of 0.05 to 0.3 g cm^{-2} yr^{-1} for the MAR, 10 to 45 dpm g^{-1} for Pb_0, 2 to 30 cm^2 yr^{-1} for DB_0 and 1 to 6 cm for x_B. The ranges were chosen based on initial test runs and literature values. The goodness of fit of each configuration was evaluated by the sum of least square errors between modeled and measured $^{210}Pb_{ex}$ and ^{137}Cs data. The average of the ten configurations with the minimum sum of least square errors was used as an approximation for the MAR, Pb_0, DB_0 and x_B values. In a second step, this configuration was further fine-tuned by visually fitting the measured data, with an emphasis on fitting the exact position of the ^{137}Cs peak. The model results and best-fit values of the adjustable variables are summarized in Table 2. The model simulations were run using the partial differential equation solver implemented in Mathematica 12.2. Mass conservation was > 99 % in all model runs.

3.3.5 Uncertainty assessment of the MAR calculations

The MAR calculation of the upper sediment section depended on the measured dry sediment weight, the surface area of the sediment core and the depth of the time marker peaks. The utilized weight scale was a Sartorius precision weight scale 120S with a measurement uncertainty of less than 0.02% relative standard deviation (RSD). A 2% RSD was employed for the surface area of the sediment cores following Sanchez-Cabeza and Ruiz-Fernández (2012). Given that the time marker activities or concentrations were measured at every centimeter, we assumed an uncertainty of 0.5 centimeters for the peak position, which relates to a 2.2 - 4.0% RSD between the different stations. Total uncertainties were propagated as follows:

$$u(\mathrm{MAR_{top}}) = \mathrm{RSD_{wt}} + \mathrm{RSD_{area}} + \mathrm{RSD_{depth}} \quad (7)$$

Where $u(MAR_{top})$ is the uncertainty of MARs in the upper sediment section and RSD_{wt}, RSD_{area} and RSD_{depth} are the uncertainties of the weight scale, surface area of the sediment core and depth of the time marker peak, respectively. In total, the uncertainty of the calculated MARs in the upper sediment section was 4.2 - 6.0% RSD or 0.006 – 0.009 g cm^{-2} yr^{-1}.

The MARs in the upper section were further dependent on how bioturbation affects the solid phase profiles of the time markers. Bioturbation was simulated using a reaction transport model (Eq. 3 - 7). The uncertainties of the MARs resulting from the model simulations were determined by the standard error between the modeled and measured ^{210}Pb data and the uncertainty of the ^{210}Pb decay constant. Total uncertainties were then propagated as follows:

$$u(\mathrm{MAR_{rtm}}) = \mathrm{RSE_{model}} + \mathrm{RSD_{\lambda}} \quad (8)$$

Where $u(MAR_{rtm})$ is the uncertainty of MARs in the upper section using the reaction transport model, RSE_{model} is the relative standard error of the modeled ^{210}Pb data and RSD_{λ} is the RSD of the decay constant λ, which is 0.5% (Sanchez-Cabeza and Ruiz-Fernández, 2012). The relative standard error between modeled and measured ^{210}Pb data varied between 9 and 24 %RSE at the different stations, resulting in a total uncertainty of 9 - 25% RSD or 0.007 - 0.026 g cm^{-2} yr^{-1}.

The uncertainty of the MAR calculation in the lower sediment section was dependent on the standard error of the linear regression and the uncertainty of the ^{210}Pb decay (Sanchez-Cabeza and Ruiz-Fernández, 2012):

$$u(MAR_{bottom}) = MAR * \sqrt{\left(\frac{u(LR)}{LR}\right)^2 + \left(\frac{u(\lambda)}{\lambda}\right)^2} \quad (9)$$

Where $u(MAR_{bottom})$ is the uncertainty of the MAR in the lower sediment section, LR and u(LR) are the linear regression and the standard error of the linear regression, respectively, λ is the ^{210}Pb decay constant (0.03118 yr^{-1}) and u(λ) is the uncertainty of the decay constant (0.00017 yr^{-1}). The resulting uncertainty of MARs in the lower section varied between 5.0 and 6.2% RSD or 0.006 - 0.015 g cm^{-2} yr^{-1}. The MARs uncertainties at each station are summarized in Table 2.

4. Results

4.1 Sedimentological and geochemical characteristics

The porosity ranged from 0.73 to 0.90, with a general decrease observed with sediment depth (Fig. 3). The sediments mainly consisted of fine-grained material with mean D_{50} values ranging from 7 to 14 µm (Tab. 1). Grain size distributions remain stable with sediment depth and time in MUC2 and MUC8. In MUC5, MUC7 and MUC9 multiple intervals with slightly coarser sediment occur, with D_{50} values between 20 and 40 µm (Fig. 4a, b).

The activity or concentration profiles of the time markers ^{137}Cs, Hg and $F^{14}C$ showed coinciding peaks situated between 10 and 25 cm sediment depth (Fig. 5). At certain stations, the Hg data showed two additional peaks at sediment depths below the main peak, most pronounced at station MUC2.

Activities of $^{210}Pb_{ex}$ generally decreased exponentially with sediment depth until reaching values close to zero (Fig. 5). In the upper 5 - 10 cm, the activities tended to be more constant. In depth intervals between 10 and 25 cm, the profiles did not follow the expected exponential decline with sediment depth but showed slightly elevated values.

4.2 Mass accumulation rates and mixing

The MARs in the upper core section calculated from the total accumulated dry sediment masses ranged from 0.11 to 0.22 g cm^{-2} yr^{-1} and the MARs determined by the reaction transport model that considers the effect of bioturbation ranged from 0.06 to 0.14 g cm^{-2} yr^{-1} (Tab. 2, Fig. 6). Sediment mixing by active bioturbation was limited to the upper 5 - 15 cm in the model with bioturbation coefficients (D_{B0}) and mixing coefficients (x_B) of 4.0 - 9.5 cm^2 yr^{-1} and 3.0 - 5.0 cm, respectively

(Tab. 2, Fig. S3). The average root mean square error (RMSE) between simulated and measured data for $^{210}Pb_{ex}$, ^{137}Cs, Hg and $F^{14}C$ were 1.1 dpm g^{-1}, 0.11 dpm g^{-1}, 8.92 μg kg^{-1} and 0.04, respectively.

In the deeper section, the MARs based on CFCS modeling ranged from 0.11 to 0.30 g cm^{-2} yr^{-1}. (Tab. 2, Fig. 6). Linear regression fits of logarithmic $^{210}Pb_{ex}$ and mass depth plots showed R^2 between 0.92 and 0.97 (Fig. 2).

On average across the stations, the MAR decreased from 0.17±0.01 to 0.14±0.01 (dry sediment mass approach) or 0.09±0.02 (reaction transport model) g cm^{-2} yr^{-1}.

5. Discussion

5.1 Modeling MARs in the Skagerrak basin

In the extensive literature, MARs have been frequently obtained using ^{210}Pb data, which can then be constrained by time markers such as ^{137}Cs. Following this approach, substantial discrepancies were identified between ^{210}Pb-derived ages and the peak position of the time marker triplet in the upper sediment section. It is likely that this offset is the result of bioturbation modifying the distribution of ^{210}Pb in surface sediments, thereby complicating the age determination using the CRS, CIC and CFCS models. Here, we suggest an alternative methodology for quantifying the temporal evolution in MARs, which involves dividing the sediment cores into two sections, separated by the depth at which the peaks of the time marker triplet were identified. Hence, the temporal variability of the MAR is depicted as a single change in 1963. However, it should be noted that this specified setup does not resolve the actual temporal evolution of the MAR in the Skagerrak basin but can only be interpreted as a net trend over the last 110 years. In order to increase the temporal resolution of the MAR variability, we recommend verifying this trend by considering further age-depth parameters, such as time markers for years other than 1963.

5.1.1 Time marker triplet for the year 1963

The activity and concentration peaks of ^{137}Cs, $F^{14}C$ and Hg served as time markers in the sediment core to derive age-depth relationships and MARs in the upper core sections. The main Hg peak and the two minor peaks at greater sediment depths were likely the result of its intense usage and production during industrialization, which were progressively regulated from 1960 to 1970 (Leipe et al., 2013; Moros et al., 2017; Polovodova Asteman et al., 2018). Two events, the nuclear bomb tests in 1963 and the Chernobyl reactor accident in 1986, released substantial amounts of ^{137}Cs and $F^{14}C$ into the atmosphere that can be traced in marine sediments. Given the correlation with the Hg peaks, the ^{137}Cs and $F^{14}C$ peaks detected in our sediment cores were attributed to the bomb tests in 1963. This is consistent with previous studies in the Skagerrak (van Weering et al., 1993; Deng et al., 2020) and in the Baltic Sea (Moros et al., 2017). Hence, the time marker triplet allowed for a robust depth assignment for the year 1963 in all sediment cores. Since the peak positions between the time markers slightly differed in the same core, we focused on the ^{137}Cs data, because this parameter has often been used in previous studies in the Skagerrak (van Weering et al., 1993; Paetzel et al., 1994; Beks, 2000; Deng et al., 2020).

5.1.2 Age-depth modeling with $^{210}Pb_{ex}$

Currently, several methods exist to determine age-depth relationships based on $^{210}Pb_{ex}$, including the constant initial activity (CIC), constant rate of supply (CRS) and constant flux and constant sedimentation (CFCS) models (Krishnaswamy et al., 1971; Robbins and Edgington, 1975; Appleby and Oldfieldz, 1983; Sanchez-Cabeza and Ruiz-Fernández, 2012; Foucher et al., 2021). In principle, CRS assumes a constant flux of $^{210}Pb_{ex}$ to the seafloor whereas CIC assumes a constant activity of $^{210}Pb_{ex}$ in particles settling to the seafloor. The CFCS approach extends these models and further assumes a constant MAR during certain periods that can be derived from linear regression analysis of logarithmic $^{210}Pb_{ex}$ activity and mass depth plots. Whether a certain model is applicable is usually determined by knowledge of the environmental system and relationships between the MAR, down-core integrated $^{210}Pb_{ex}$ values and $^{210}Pb_{ex}$ activities in settling particles (Appleby and Oldfieldz, 1983; Sanchez-Cabeza and Ruiz-Fernández, 2012). Although the amount of data presented in this study only allowed a limited evaluation, reasonably linear relationships between the logarithmic $^{210}Pb_{ex}$ and mass depth data below the time marker peaks (Fig. 2) indicate that the application of the CFCS model is valid in this depth interval. It should be noted, however, that the elevated activities between 10 and 25 cm in the $^{210}Pb_{ex}$ profiles affected the linear regression fits. It is possible that the additional $^{210}Pb_{ex}$ in this depth interval may not be the result of sedimentation processes, but may rather be the consequence of excess production of ^{210}Pb in the atmosphere during the nuclear bomb testing in 1963 (Jaworowski, 1966; Jaworowski et al., 1978). However, this hypothesis is controversial, as other studies did not observe elevated ^{210}Pb values in samples measured during this period (Bhandari et al., 1966; Crozaz, 1966). If nuclear weapon tests did indeed introduce significant amounts of ^{210}Pb into the atmosphere, then the MAR before 1963 might have been underestimated to some extent. The MARs in the deep section below the time marker peaks are applicable to the time interval from 1963 to ~ 1911 (i.e. 110 years before sediment core retrieval in 2021), as roughly 97% of the $^{210}Pb_{ex}$ is decayed after five times its half-life (22.3 years). The $^{210}Pb_{ex}$ data was further employed alongside the time markers in the upper sediment section to simulate the effects of bioturbation on the solid phase profiles using a reaction transport model (Eq. 3 - 7). Therefore, a constant ^{210}Pb activity was set at the upper boundary of the sediment column to describe the settling of $^{210}Pb_{ex}$ at the seafloor (Eq. 7), in accordance with the concept of the CIC model. The CIC method is generally recommended when variable sources of $^{210}Pb_{ex}$ are present (Sanchez-Cabeza and Ruiz-Fernández, 2012) and sediment focusing occurs (Appleby and Oldfieldz, 1983). This is the case in the Skagerrak marked by a significant lateral input of $^{210}Pb_{ex}$ and high sedimentation rates along the deeper basin where our stations are located (De Haas and van Weering, 1997; Spiegel et al., 2024a). Furthermore, the CIC model generally yielded better fits to the data than the CRS model in the surface sediments, which is why we selected the CIC model to simulate the $^{210}Pb_{ex}$ profiles.

5.1.3 Effect of bioturbation on the MAR

In addition to the simple dry sediment mass approach, we set up a reaction transport model including a biodiffusion formulation (Eq. 3) to predict the effect of bioturbation on the solid phase profiles. To showcase the principle impact of bioturbation on the depth distribution of the time marker ^{137}Cs, we compared the results of the model run with the bioturbation parameterization that led to the best fit to the measured data (Tab. 2) to a run using the same MAR but excluding bioturbation in the simulation (Fig. 7). In addition to a broadening of the ^{137}Cs signal, the comparison reveals that the peak position of the time marker is located ~ 4 cm deeper into the sediment in the model run including bioturbation. In other words, bioturbation pushes down the time marker peak deeper into the sediment so that a lower MAR is required in the model runs to fit the time marker profile. Such downward transportation of solids due to bioturbation has been suggested in previous studies (Crusius et al., 2004; Crusius and Kenna, 2007; Hülse et al., 2022). As a result, the MARs in the upper core section derived from the reaction transport model were systemically lower compared to the dry sediment mass approach across the stations. Consequently, the decline in the MAR in the Skagerrak basin over time is more pronounced if bioturbation is considered. Nevertheless, it is yet unclear whether the biodiffusion formulation in our model and the resulting push-down effect accurately reflect the natural conditions in Skagerrak sediments. It is possible that the effect of bioturbation on solid phase profiles can be minimised by analysing sediment cores taken in the northeastern Skagerrak, where higher MARs have been reported than in the central Skagerrak basin (Erlenkeuser and Pederstad, 1984; van Weering et al., 1987, 1993; Meyenburg and Liebezeit, 1993). However, the sediments in this area are more likely to have been affected by anthropogenic mixing, such as bottom trawling, as evidenced by the disturbed ^{210}Pb profiles observed in a previous study (Spiegel et al., 2023).

The bioturbation coefficients at the sediment surface (D_{B0}) of 4.0 - 9.5 cm^2 yr^{-1} derived from our model results (Tab. 2) fall within the range of global estimates at comparable MARs (Boudreau, 1997). However, they are higher compared to 1.0 - 2.0 cm^2 yr^{-1} presented in an earlier study based on chlorophyll-a measurements and observations of the faunal community structure in the same area (Deng et al., 2020). The difference likely arises due to the different approaches to derive bioturbation parameters and the heterogeneity of the Skagerrak seafloor. Therefore, the results of the reaction transport model likely represent an upper limit of the MAR in the upper core section if the chosen biodiffusion description in the model adequately represents the natural system. Conversely, the MAR determined from the sum of the dry sediment mass above the time marker peak (Eq. 1) might represent a lower limit. Based on the available data, it was not possible to determine the depth distribution of bioturbation intensities with an independent parameter to constrain the model results, i.e. by direct or further particle tracer methods (Maire et al., 2008). Given that the degree of the MAR decline strongly depends on how bioturbation affects the solid phase distributions in Skagerrak sediments, a better understanding of bioturbation in marine sediments and its implementation into environmental models would significantly improve the validity of our results.

5.2. Change in the MAR in 1963

The major finding of this study is a general decreasing trend in the MAR in the Skagerrak basin over time, with average MARs decreasing from 0.17±0.01 to 0.14±0.01 g cm^{-2} yr^{-1} before and after 1963 (Tab. 2, Fig. 6). A larger MAR decrease from 0.17±0.01 to 0.09±0.02 g cm^{-2} yr^{-1} is obtained if bioturbation in the upper sediment section is considered and affects the solid phase profiles as simulated by the reaction transport model. It is important to note that the MARs reflect sedimentation conditions in the deep and central Skagerrak basin and are not representative of shallower areas. The Skagerrak basin is characterized by low current velocities, comparably stagnant waters, fine-grained sediments and the suspended material is likely transported from the northern Atlantic into the deeper Skagerrak (Ljøen and Svansson, 1972; Thiede, 1985; Rodhe, 1996; Rodhe and Holt, 1996). In contrast, sedimentation at shallower water depths is characterized by a more energetic milieu, the deposition of coarser material and erosional areas (Bergsten et al., 1996; Bøe et al., 1996; Stevens et al., 1996). Hence, MARs at shallower water depths in the Skagerrak might exhibit different temporal trends.

The presented MARs are of similar magnitude as those previously obtained in the Skagerrak region (Erlenkeuser and Pederstad, 1984; van Weering et al., 1987, 1993; Ståhl et al., 2004; Deng et al., 2020; Spiegel et al., 2024a). However, in many cases sediment deposition in the Skagerrak has been presented as a steady-state process or age-depth reconstructions have been based solely on the use of $^{210}Pb_{ex}$. Hence, this study indicates a potential degree of uncertainty in some of the existing literature and a change in the MARs should be considered when interpreting transient features in the benthic Skagerrak environment. For instance, accumulation rates of benthic foraminifera have been shown to increase after 1970 along with a species shift in the Skagerrak basin (Alve, 1996). However, the reason for this shift could not be conclusively determined. A decline in the MARs over time as presented in our study could have attenuated the effect of sediment dilution on benthic foraminifera abundancies, while also potentially shifting the ecological conditions to benefit certain species. Hence, the decrease in MARs may provide a plausible explanation for the observed increase in benthic foraminifera accumulation rates.

On a larger scale, previous studies estimated sediment deposition in the Skagerrak to account for 45 - 80 % of the total sediment inputs into the North Sea (Oost et al., 2021; Spiegel et al., 2024a). Furthermore, a substantial proportion of the Skagerrak deposits (~76 %) likely originate from the North Sea (De Haas and van Weering, 1997; Spiegel et al., 2024a). Considering that our study reveals a net decreasing trend in the MAR, it is reasonable to infer that the North Sea sediment system might have been subject to significant change in the period from 1900 to 2021.

5.3 Driving factors for the temporal variability of the MAR

Prior to our study, we anticipated to find a MAR increase in the Skagerrak basin over the last decades since bottom trawling, sediment extraction and other human activities disturb the seabed and resuspend surface sediments, increasing the particle load in the North Sea water column (De Groot, 1986; Baeye and Fettweis, 2015; Eigaard et al., 2017; ICES, 2019; Mielck et al., 2019; Slavik et al., 2019; ICES, 2020; Rijnsdorp et al., 2020; Daewel et al., 2022; Heinatz and Scheffold, 2023). Similarly, climate change-related variability in temperature, precipitation and sea level rise in the North Sea region (Wahl et al., 2013) likely enhanced sediment inputs by elevated coastal erosion rates, as has been shown along the Holderness coastline (Pye and Blott, 2015). Since part of the additional suspended material is transported to the Skagerrak, such human and natural processes should theoretically lead to an increase of MARs in the Skagerrak. However, we did not observe such an increase but a substantial MAR decrease since 1963 in the deep Skagerrak basin. Hence, other factors that outweigh the above human and natural processes are required to explain our unexpected observation.

River dams have been progressively constructed in the major North Sea rivers and their tributaries, that is, the Elbe, Weser and Ems rivers (IKSE, 2005; Lange et al., 2008; IKSE, 2012; Hübner and Schwandt, 2018) and their harbour and estuary channels have been deepened numerous times (Goelz, 2008; KFKI, 2008; Marusic, 2008). Such human measures typically reduce the riverine particle discharge into the ocean (Syvitski et al., 2005; Ericson et al., 2006; Graf, 2006; Goelz, 2008). Considering that riverine discharge represents ~ 5 - 11 % of the total sediment inputs into the North Sea (Eisma and Irion, 1988; Oost et al., 2021) and similar human alterations in other river systems have been previously linked to substantial decreases in riverine sediment transport (Williams and Wolman, 1984; Walling and Fang, 2003), river damming and the deepening of harbour and estuary channels may have reduced the particle load into the North Sea. Furthermore, extensive parts of the North Sea coastline have been protected against erosion by dykes, wave breaks, land reclamation and other coastal protection means (Kelletat, 1992; Hoeksema, 2007; Hofstede, 2008), such as the Delta

Works project in the Netherlands that started in 1954 (Hillen et al., 1993). Coastal erosion has been estimated to contribute ~ 3 - 9 % of the total sediment inputs in the North Sea (Eisma and Irion, 1988; Puls et al., 1997; Oost et al., 2021). However, recent studies suggested that coastal erosion rates might be underestimated in the North Atlantic (Regard et al., 2022) and in the Baltic Sea (Wallmann et al., 2022). Consequently, human interventions in rivers and at coastlines may have substantially reduced the sediment budget of the North Sea and could therefore represent major driving factors for the observed MAR decline in the Skagerrak.

Approximately 14 - 25 % of the total suspended solids entering the North Sea are deposited in the Wadden Sea, making it a major sink for sediments (Oost et al., 2021). Previous studies have suggested that a combination of relative sea level rise, circulation patterns and redistribution of sediments may have increased accretion rates in the Wadden Sea over time (Cahoon et al., 2000; van Wijnen and Bakker, 2001; Flemming, 2002; Madsen et al., 2007; Bartholdy et al., 2010; Schindler et al., 2014), while other observations indicated a loss of sediments in certain areas (Flemming and Nyandwi, 1994; Mai and Bartholomä, 2000; van Wijnen and Bakker, 2001; Flemming, 2002). Ultimately, it remains unclear how the sediment input across the entirety of the Wadden Sea region has changed over time. Given the substantial deposition in the Wadden Sea, it is feasible that less material would be available for transportation and subsequent deposition in the Skagerrak if accretion rates in the Wadden Sea gradually increased over time.

Variations in the circulation system have been previously discussed to influence sediment dynamics in the North Sea and Skagerrak (Nordberg, 1991; Bøe et al., 1996; Filipsson and Nordberg, 2004; Gyllencreutz et al., 2006). The hydrography of the North Sea reveals three major transportation pathways for water and sediment from the northern Atlantic to the Skagerrak (Fig. 1b). Previous studies demonstrated that the variability in the circulation system of the North Sea correlates with the North Atlantic Oscillation (NAO) and wind conditions (Mathis et al., 2015; Daewel and Schrum, 2017). They show that before 1960, weaker westerly wind conditions likely diminished the water inflow through the northern entrance, thereby enhancing the Dooley Current, which supplies the Tampen Bank Current and the Central North Sea Current. These currents transport material on a direct pathway to the Skagerrak, which could explain higher MARs in the Skagerrak prior to 1963. Between 1970 and 2000 a positive NAO phase and strong westerly winds fostered the southward transport along the British coastline. During this period, a larger proportion of the sediment was likely transported along the elongated pathway through the southern North Sea and across the depocenter of the Wadden Sea where the sediment could settle before reaching the Skagerrak. Given that 13 - 43 % of the total sediment input is delivered through the northern entrance (Oost et al., 2021) and 43% of the Skagerrak deposits stem from the northern North Sea (Lenz et al., 2024), the temporal variability in the hydrography and its effect on the amount of sediment that reaches the Skagerrak may have contributed to the MAR decline in the Skagerrak.

Storm events occur frequently in the North Sea (Dangendorf et al., 2014) and redistribute sediments (Green et al., 1995; Stanev et al., 2009; Fettweis et al., 2010). Since particle settling is dependent on the energetic conditions in the water column (Hjulstrom, 1939; McCave and Swift, 1976), grain size records have been used as proxies for past storm activity in the Skagerrak (Hass, 1996). Accordingly, sharp layers with notably coarser grain sizes at MUC5, MUC7 and MUC9 (Fig 4a, b) are likely the result of storm events. However, no clear trends in the frequency or shape of the grain size peaks with sediment depth or time were observed across the stations. Hence, although storm events left traces in the grain size distribution in the Skagerrak, they were likely not responsible for the declining long-term trend in the MAR.

It should be noted that our dataset only allowed for a qualitative assessment of the different drivers behind the decrease in MARs in the Skagerrak basin. At the present stage, it is challenging to attribute the decrease in the MARs in the deep Skagerrak basin to natural or human processes. Furthermore, it was not possible to derive conclusions for the shallow areas from our study, as sedimentation processes in the deep and shallow Skagerrak differ significantly. Nevertheless, the finding that MARs changed in the deep basin is an intriguing finding in its own right. The overview of potential driving factors can serve as a basis for future quantitative analysis of the sediment cycle in the North Sea. We recommend integrating the different driving mechanisms into non-steady state particle transport models to further explore the temporal evolution of the sediment cycle. Our presented MAR data can then be used to validate such models in combination with additional field data on the temporal evolution of the provenance, transport pathways and deposition of sediments in the Skagerrak and North Sea.

6. Conclusion

Based on comparing the MAR before and after 1963 at six sediment cores in the deep Skagerrak basin, we determined that the MAR on average decreased from 0.17 to 0.14 g cm^{-2} yr^{-1}. If bioturbation is considered and affects the solid phase as described by the commonly used biodiffusive model description, then the MAR after 1963 is significantly lower at 0.09 g cm^{-2} yr^{-1}. Hence, the temporal variability of the MAR not only depends on the validity of the age-depth model but also on bioturbation rates in Skagerrak sediments and their implementation in models. To verify our results, we therefore recommend examining additional age-depth parameters, particularly time markers for years other than 1963 and improving our understanding of bioturbation in the Skagerrak, i.e. by independent tracer studies. Considering that the Skagerrak represents the largest depocenter for sediments from the North Sea, the decline in the MAR suggests that the sediment system of the North Sea has been subject to substantial change during the last 110 years. We summarized major processes that potentially shifted the sediment cycle of the North Sea leading to a decrease in the MAR in the Skagerrak basin:

- River damming, deepening of harbour channels and coastal protection decreased the suspended sediment input into the North Sea
- A change in the North Sea circulation pattern reduced the amount of sediment transported to the Skagerrak
- Increased sediment deposition in other North Sea depocenters such as the Wadden Sea

These factors are likely to have outweighed processes that would theoretically increase Skagerrak deposition rates, such as resuspension triggered by human activities and storm events, temperature, humidity and sea level rise. However, a quantitative evaluation of the different contributors to sediment deposition in the Skagerrak is necessary to better describe the temporal change in the sediment system of the North Sea.

Data availability statement

The sedimentary data of ^{210}Pb, ^{137}Cs, $F^{14}C$ and Hg are stored in the PANGAEA database https://doi.org/10.1594/PANGAEA.967080 (Spiegel et al., 2024b).

Funding source

Funding for this study was provided by the Federal Ministry of Education and Research, Germany, via the APOC project (03F0874B) – "Anthropogenic impacts on particulate organic carbon cycling in the North Sea".

Acknowledgements

We wish to thank the captain and the crew of RV Alkor for their support onboard the RV Alkor during the cruise AL561, as well as our colleagues Bettina Domeyer, Anke Bleyer, Regina Surberg, Matthias Türk and Asmus Petersen for their help onboard and in the GEOMAR laboratories. We acknowledge the “Gutachter Panel Forschungsschiffe” (GPF 21-2_028, APOC) for support to realize the AL561 cruise. We also thank Andreas Neumann from the Helmholtz-Zentrum Hereon for providing sediment samples of St.65 from the RV Alkor cruise AL557. We would further like to acknowledge Bernd Kopka and Marvin Blaue from the Laboratory for Radioisotopes at the University of Göttingen and Christian Kunze and Robert Arndt from the IAF Dresden for the ^{210}Pb and ^{137}Cs analyses. We are further thankful for ^{14}C measurements performed by Gesine Mollenhauer and her team at Alfred Wegener Institute Helmholtz Centre for Polar and Marine Research.

Literature

Aller, R.C., 1982. The Effects of Macrobenthos on Chemical Properties of Marine Sediment and Overlying Water, in: McCall, P.L., Tevesz, M.J.S. (Eds.), Animal-Sediment Relations, Topics in Geobiology. Springer US, Boston, MA, pp. 53–102. https://doi.org/10.1007/978-1-4757-1317-6_2

Alve, E., 1996. Benthic foraminiferal evidence of environmental change in the Skagerrak over the past six decades. Nor. geol. unders. Bull. 430, 85–93.

Appleby, P.G., Oldfieldz, F., 1983. The assessment of 210Pb data from sites with varying sediment accumulation rates. Hydrobiologia 103, 29–35. https://doi.org/10.1007/BF00028424

Axe, P., Clausen, U., Leujak, W., Malcolm, S., Ruiter, H., Prins, T., Harvey, E.T., 2017. Eutrophication Status of the OSPAR Maritime Area. Third Integrated Report on the Eutrophication Status of the OSPAR Maritime Area.

Baeye, M., Fettweis, M., 2015. In situ observations of suspended particulate matter plumes at an offshore wind farm, southern North Sea. Geo-Mar. Lett. 35, 247–255. https://doi.org/10.1007/s00367-015-0404-8

Bartholdy, A.T., Bartholdy, J., Kroon, A., 2010. Salt marsh stability and patterns of sedimentation across a backbarrier platform. Mar. Geol. 278, 31–42. https://doi.org/10.1016/j.margeo.2010.09.001

Beks, J.P., 2000. Storage and distribution of plutonium, 241Am, 137Cs and 210Pbxs in North Sea sediments. Cont. Shelf Res. 20, 1941–1964. https://doi.org/10.1016/S0278-4343(00)00057-1

Bergsten, H., Nordberg, K., Malmgren, B., 1996. Recent benthic foraminifera as tracers of water masses along a transect in the Skagerrak, north-eastern North Sea. J. Sea Res. 35, 111–121. https://doi.org/10.1016/S1385-1101(96)90740-6

Berner, R.A., 1980. Early diagenesis: a theoretical approach, Princeton series in geochemistry. Princeton University Press, Princeton, N.J.

Bhandari, N., Lal, D., Rama, D., 1966. Stratospheric circulation studies based on natural and artificial radioactive tracer elements. Tellus 18 (2–3), 391–406.

Bjørnstad, H., Salbu, B., Rosenqvist, I.Th., 1985. Uranium concentrations in Upper Quaternary Skagerrak deposits. Nor. J. Geol. 65, 1, 2.

Blott, S.J., Pye, K., 2001. GRADISTAT: a grain size distribution and statistics package for the analysis of unconsolidated sediments. Earth Surf. Process. Landf. 26, 1237–1248. https://doi.org/10.1002/esp.261

Bøe, R., Rise, L., Thorsnes, T., Haas, de, Sæther, O., Kunzendorf, H., 1996. Sea-bed sediments and sediment accumulation rates in the Norwegian part of Skagerrak. Nor. Geol. Unders. Bull 75.

Boudreau, B.P., 1997. Diagenetic models and their implementation: modelling transport and reactions in aquatic sediments. Springer, Berlin.

Boudreau, B.P., 1986. Mathematics of tracer mixing in sediments; II, Nonlocal mixing and biological conveyor-belt phenomena. Am. J. Sci. 286, 199–238. https://doi.org/10.2475/ajs.286.3.199

Bradshaw, C., Jakobsson, M., Brüchert, V., Bonaglia, S., Mörth, C.-M., Muchowski, J., Stranne, C., Sköld, M., 2021. Physical Disturbance by Bottom Trawling Suspends Particulate Matter and Alters Biogeochemical Processes on and Near the Seafloor. Front. Mar. Sci. 8, 683331. https://doi.org/10.3389/fmars.2021.683331

Butzin, M., Sidorenko, D., Köhler, P., 2021. A multi-resolution ocean simulation of the anthropogenic radiocarbon transient (other). pico. https://doi.org/10.5194/egusphere-egu21-3118

Butzin, M., Ye, Y., Völker, C., Gürses, Ö., Hauck, J., Köhler, P., 2023. Carbon isotopes in the marine biogeochemistry model FESOM2.1-REcoM3 (preprint). Climate and Earth system modeling. https://doi.org/10.5194/egusphere-2023-1718

Cahoon, D.R., French, J.R., Spencer, T., Reed, D., Möller, I., 2000. Vertical accretion versus elevational adjustment in UK saltmarshes: an evaluation of alternative methodologies. Geol. Soc. Lond. Spec. Publ. 175, 223–238. https://doi.org/10.1144/GSL.SP.2000.175.01.17

Conradsen, K., Bergsten, H., Knudsen, K.L., Nordberg, K., Seidenkrantz, M.-S., 1994. RECENT BENTHIC FORAMINIFERAL DISTRIBUTION IN THE KATTEGAT AND THE SKAGERRAK, SCANDINAVIA, in: Sejrup, H.P., Knudsen, K.L. (Eds.), Late Cenozoic Benthic Foraminifera: Taxonomy, Ecology and Stratigraphy. In Honour of Rolf W. Feyling-Hanssen on His 75th Birthday. July 24, 1993. Cushman Foundation for Foraminiferal Research, p. 0.

Crozaz, G., 1966. Dating of Glaciers by Lead-210. Symp Radioact. Dating Methods Low-Level Count. 385.

Crusius, J., Bothner, M.H., Sommerfield, C.K., 2004. Bioturbation depths, rates and processes in Massachusetts Bay sediments inferred from modeling of 210Pb and 239+240Pu profiles. Estuar. Coast. Shelf Sci. 61, 643–655. https://doi.org/10.1016/j.ecss.2004.07.005

Crusius, J., Kenna, T.C., 2007. Ensuring confidence in radionuclide-based sediment chronologies and bioturbation rates. Estuar. Coast. Shelf Sci. 71, 537–544. https://doi.org/10.1016/j.ecss.2006.09.006

Daewel, U., Akhtar, N., Christiansen, N., Schrum, C., 2022. Offshore wind farms are projected to impact primary production and bottom water deoxygenation in the North Sea. Commun. Earth Environ. 3, 292. https://doi.org/10.1038/s43247-022-00625-0

Daewel, U., Schrum, C., 2017. Low-frequency variability in North Sea and Baltic Sea identified through simulations with the 3-D coupled physical–biogeochemical model ECOSMO. Earth Syst. Dyn. 8, 801–815. https://doi.org/10.5194/esd-8-801-2017

Dale, A.W., Paul, K.M., Clemens, D., Scholz, F., Schroller-Lomnitz, U., Wallmann, K., Geilert, S., Hensen, C., Plass, A., Liebetrau, V., Grasse, P., Sommer, S., 2021. Recycling and Burial of Biogenic Silica in an Open Margin Oxygen Minimum Zone. Glob. Biogeochem. Cycles 35. https://doi.org/10.1029/2020GB006583

Dangendorf, S., Müller-Navarra, S., Jensen, J., Schenk, F., Wahl, T., Weisse, R., 2014. North Sea Storminess from a Novel Storm Surge Record since AD 1843*. J. Clim. 27, 3582–3595. https://doi.org/10.1175/JCLI-D-13-00427.1

Danilov, S., Sidorenko, D., Wang, Q., Jung, T., 2017. The Finite-volumE Sea ice–Ocean Model (FESOM2). Geosci. Model Dev. 10, 765–789. https://doi.org/10.5194/gmd-10-765-2017

De Groot, S.J., 1986. Marine sand and gravel extraction in the North Atlantic and its potential environmental impact, with emphasis on the North Sea. Ocean Manag. 10, 21–36. https://doi.org/10.1016/0302-184X(86)90004-1

De Haas, H., van Weering, T.C.E., 1997. Recent sediment accumulation, organic carbon burial and transport in the northeastern North Sea. Mar. Geol. 136, 173–187. https://doi.org/10.1016/S0025-3227(96)00072-2

Deng, L., Bölsterli, D., Kristensen, E., Meile, C., Su, C.-C., Bernasconi, S.M., Seidenkrantz, M.-S., Glombitza, C., Lagostina, L., Han, X., Jørgensen, B.B., Røy, H., Lever, M.A., 2020. Macrofaunal control of microbial community structure in continental margin sediments. Proc. Natl. Acad. Sci. 117, 15911–15922. https://doi.org/10.1073/pnas.1917494117

Eigaard, O.R., Bastardie, F., Hintzen, N.T., Buhl-Mortensen, L., Buhl-Mortensen, P., Catarino, R., Dinesen, G.E., Egekvist, J., Fock, H.O., Geitner, K., Gerritsen, H.D., González, M.M., Jonsson, P., Kavadas, S., Laffargue, P., Lundy, M., Gonzalez-Mirelis, G., Nielsen, J.R., Papadopoulou, N., Posen, P.E., Pulcinella, J., Russo, T., Sala, A., Silva, C., Smith, C.J., Vanelslander, B., Rijnsdorp, A.D., 2017. The footprint of bottom trawling in European waters: distribution, intensity, and seabed integrity. ICES J. Mar. Sci. 74, 847–865. https://doi.org/10.1093/icesjms/fsw194

Eisma, D., Irion, G., 1988. Suspended Matter and Sediment Transport, in: Salomons, W., Bayne, B.L., Duursma, E.K., Förstner, U. (Eds.), Pollution of the North Sea. Springer Berlin Heidelberg, Berlin, Heidelberg, pp. 20–35. https://doi.org/10.1007/978-3-642-73709-1_2

Elliott, M., Nedwell, S., Jones, N.V., Read, S.J., Cutts, N.D., Hemingway, K.L., 1998. Intertidal Sand and Mudflats & Subtidal Mobile Sandbanks (volume II). An overview of dynamic and sensitivity characteristics for conservation management of marine SACs. Scott. Assoc. Mar. Sci. UK Mar. SACs Proj.

Ericson, J., Vorosmarty, C., Dingman, S., Ward, L., Meybeck, M., 2006. Effective sea-level rise and deltas: Causes of change and human dimension implications. Glob. Planet. Change 50, 63–82. https://doi.org/10.1016/j.gloplacha.2005.07.004

Erlenkeuser, H., 1985. Distribution of 210Pb with depth in core GIK 15530-4 from the Skagerrak. Nor. Geol. Tidsskr. 65, 27–34.

Erlenkeuser, H., Pederstad, K., 1984. Recent sediment accumulation in Skagerrak as depicted by 210pb-dating. Nor. Geol. Tidsskr. 18.

Fettweis, M., Francken, F., Van Den Eynde, D., Verwaest, T., Janssens, J., Van Lancker, V., 2010. Storm influence on SPM concentrations in a coastal turbidity maximum area with high anthropogenic impact (southern North Sea). Cont. Shelf Res. 30, 1417–1427. https://doi.org/10.1016/j.csr.2010.05.001

Filipsson, H.L., Nordberg, K., 2004. Climate variations, an overlooked factor influencing the recent marine environment. An example from Gullmar Fjord, Sweden, illustrated by benthic foraminifera and hydrographic data. Estuaries 27, 867–881. https://doi.org/10.1007/BF02912048

Flemming, B.W., 2002. Effects of Climate and Human Interventions on the Evolution of the Wadden Sea Depositional System (Southern North Sea), in: Wefer, G., Berger, W.H., Behre, K.-E., Jansen, E. (Eds.), Climate Development and History of the North Atlantic Realm. Springer Berlin Heidelberg, Berlin, Heidelberg, pp. 399–413. https://doi.org/10.1007/978-3-662-04965-5_26

Flemming, B.W., Nyandwi, N., 1994. Land reclamation as a cause of fine-grained sediment depletion in backbarrier tidal flats (Southern North Sea). Neth. J. Aquat. Ecol. 28, 299–307. https://doi.org/10.1007/BF02334198

Folk, R.L., Ward, W.C., 1957. Brazos River bar [Texas]; a study in the significance of grain size parameters. J. Sediment. Res. 27, 3–26. https://doi.org/10.1306/74D70646-2B21-11D7-8648000102C1865D

Foucher, A., Chaboche, P.-A., Sabatier, P., Evrard, O., 2021. A worldwide meta-analysis (1977–2020) of sediment core dating using fallout radionuclides including ¹³⁷Cs and ²¹⁰Pb_{xs} Earth Syst. Sci. Data 13, 4951–4966. https://doi.org/10.5194/essd-13-4951-2021

Garcia Agudo, E., 1998. Global distribution of 137Cs inputs for soil erosion and sedimentation studies, in: International Atomic Energy Agency (Ed.), Use of 137Cs in the Study of Soil Erosion and Sedimentation. IAEA-TECDOC-1028 117–121.

Goelz, E., 2008. Improved sediment-management strategies for the sustainable development of german waterways. IAHS-AISH Publ. 540–549.

Graf, W.L., 2006. Downstream hydrologic and geomorphic effects of large dams on American rivers. Geomorphology 79, 336–360. https://doi.org/10.1016/j.geomorph.2006.06.022

Graven, H., Allison, C.E., Etheridge, D.M., Hammer, S., Keeling, R.F., Levin, I., Meijer, H.A.J.J., Rubino, M., Tans, P.P., Trudinger, C.M., Vaughn, B.H., White, J.W.C., 2017. Compiled records of carbon isotopes in atmospheric CO 2 for historical simulations in CMIP6. Geosci. Model Dev. 10, 4405–4417. https://doi.org/10.5194/GMD-10-4405-2017

Green, M.O., Vincent, C.E., McCave, I.N., Dickson, R.R., Rees, J.M., Pearsons, N.D., 1995. Storm sediment transport: observations from the British North Sea shelf. Cont. Shelf Res. 15, 889–912. https://doi.org/10.1016/0278-4343(95)80001-T

Gyllencreutz, R., Backman, J., Jakobsson, M., Kissel, C., Arnold, E., 2006. Postglacial palaeoceanography in the Skagerrak. The Holocene 16, 975–985. https://doi.org/10.1177/0959683606hl988rp

Hass, H.C., 1996. Northern Europe climate variations during late Holocene: evidence from marine Skagerrak. Palaeogeogr. Palaeoclimatol. Palaeoecol. 123, 121–145. https://doi.org/10.1016/0031-0182(95)00114-X

Heier-Nielsen, S., Conradsen, K., Heinemeier, J., Knudsen, K.L., Nielsen, H.L., Rud, N., Sveinbjörnsdóttir, Á.E., 1995. Radiocarbon Dating of Shells and Foraminifera from the Skagen Core, Denmark: Evidence of Reworking. Radiocarbon 37, 119–130. https://doi.org/10.1017/S0033822200030551

Heinatz, K., Scheffold, M.I.E., 2023. A first estimate of the effect of offshore wind farms on sedimentary organic carbon stocks in the Southern North Sea. Front. Mar. Sci. 9, 1068967. https://doi.org/10.3389/fmars.2022.1068967

Hiddink, J.G., Van De Velde, S.J., McConnaughey, R.A., De Borger, E., Tiano, J., Kaiser, M.J., Sweetman, A.K., Sciberras, M., 2023. Quantifying the carbon benefits of ending bottom trawling. Nature 617, E1–E2. https://doi.org/10.1038/s41586-023-06014-7

Hillen, R., Smaal, A.C., van Huijssteeden, A.J., Misdorp, R., 1993. The Dutch Delta. aspects of coastal zone management, in: Proceedings of the World Coast Conference 1993: ÔPreparing to Meet the Coastal Challenges of the 21 St centuryÕ. Coastal Zone Management Centre The Hague, pp. 653–659.

Hjulstrom, F., 1939. Transportation of detritus by moving water. PD Trask Ed Recent Mar. Sediments Am Assoc Pet. Geol. Tulsa 5–31.

Hoeksema, R.J., 2007. Three stages in the history of land reclamation in the Netherlands. Irrig. Drain. 56, S113–S126. https://doi.org/10.1002/ird.340

Hofstede, J., 2008. Coastal Flood Defence and Coastal Protection along the North Sea Coast of Schleswig-Holstein. Küste 134–142.

Holland, K.T., Elmore, P.A., 2008. A review of heterogeneous sediments in coastal environments. Earth-Sci. Rev. 89, 116–134. https://doi.org/10.1016/j.earscirev.2008.03.003

Hübner, G., Schwandt, D., 2018. EXTREME LOW FLOW AND WATER QUALITY – A LONG-TERM VIEW ON THE RIVER ELBE. Erdkunde 72, 235–252.

Hülse, D., Vervoort, P., Van De Velde, S.J., Kanzaki, Y., Boudreau, B., Arndt, S., Bottjer, D.J., Hoogakker, B., Kuderer, M., Middelburg, J.J., Volkenborn, N., Kirtland Turner, S., Ridgwell, A., 2022. Assessing the impact of bioturbation on sedimentary isotopic records through numerical models. Earth-Sci. Rev. 234, 104213. https://doi.org/10.1016/j.earscirev.2022.104213

Hylander, L.D., Meili, M., 2003. 500 years of mercury production: global annual inventory by region until 2000 and associated emissions. Sci. Total Environ. 304, 13–27. https://doi.org/10.1016/S0048-9697(02)00553-3

ICES, 2020. Greater North Sea ecoregion ? Fisheries overview, including mixed-fisheries considerations. https://doi.org/10.17895/ICES.ADVICE.7605

ICES, 2019. Working Group on the Effects of Extraction of Marine Sediments on the Marine Ecosystem (WGEXT). https://doi.org/10.17895/ICES.PUB.5733

ICES, 2018. Greater North Sea Ecoregion ? Ecosystem overview. https://doi.org/10.17895/ICES.PUB.4670

IKSE, 2012. Abschlussbericht über die Erfüllung des „Aktionsplans Hochwasserschutz Elbe“ im Zeitraum 2003–2011.

IKSE, 2005. Die Elbe und ihr Einzugsgebiet – Ein geographisch-hydrologischer und wasserwirtschaftlicher Überblick.

Jaworowski, Z., 1966. Temporal and Geographical Distribution of Radium D (Lead-210). Nature 212, 886–889. https://doi.org/10.1038/212886a0

Jaworowski, Z., Kownacka, L., Grotowski, K., Kwiatkowski, K., 1978. Lead-210 from nuclear explosions in the environment. Nucl. Technol. 37, 159–166.

Kelletat, D., 1992. Coastal Erosion and Protection Measures at the German North Sea Coast. J. Coast. Res. 8, 699–711.

Key, R.M., Kozyr, A., Sabine, C.L., Lee, K., Wanninkhof, R., Bullister, J.L., Feely, R.A., Millero, F.J., Mordy, C., Peng, T. -H., 2004. A global ocean carbon climatology: Results from Global Data Analysis Project (GLODAP). Glob. Biogeochem. Cycles 18, 2004GB002247. https://doi.org/10.1029/2004GB002247

KFKI (Ed.), 2008. Die Küste, 74 ICCE. Küste Arch. Für Forsch. Tech. Nord. Ostsee Arch. Res. Technol. North Sea Balt. Coast.

Krishnaswamy, S., Lal, D., Martin, J.M., Meybeck, M., 1971. Geochronology of lake sediments. Earth Planet. Sci. Lett. 11, 407–414. https://doi.org/10.1016/0012-821X(71)90202-0

Lange, D., Müller, H., Piechotta, F., Schubert, R., 2008. The Weser Estuary. Küste 275–287.

Large, W.G., Yeager, S.G., 2009. The global climatology of an interannually varying air–sea flux data set. Clim. Dyn. 33, 341–364. https://doi.org/10.1007/s00382-008-0441-3

Leipe, T., Moros, M., Kotilainen, A., Vallius, H., Kabel, K., Endler, M., Kowalski, N., 2013. Mercury in Baltic Sea sediments—Natural background and anthropogenic impact. Geochemistry 73, 249–259. https://doi.org/10.1016/j.chemer.2013.06.005

Lenz, N., Spiegel, T., Hathorne, E., Wallmann, K., Eisenhauer, A., Frank, M., 2024. Provenance of clay-sized detrital sediments in the North Sea and the Skagerrak region based on radiogenic Nd-Sr-Hf isotopes and clay mineral compositions: assessing the impact of coastal and seabed erosion. Front. Mar. Sci. 11, 1416519. https://doi.org/10.3389/fmars.2024.1416519

Ljøen, R., Svansson, A., 1972. Long-term variations of subsurface temperatures in the Skagerrak. Deep Sea Res. Oceanogr. Abstr. 19, 277–288. https://doi.org/10.1016/0011-7471(72)90021-6

Lodder, Wang, Elias, Van Der Spek, De Looff, Townend, 2019. Future Response of the Wadden Sea Tidal Basins to Relative Sea-Level rise—An Aggregated Modelling Approach. Water 11, 2198. https://doi.org/10.3390/w11102198

Lohmann, G., Butzin, M., Eissner, N., Shi, X., Stepanek, C., 2020. Abrupt Climate and Weather Changes Across Time Scales. Paleoceanogr. Paleoclimatology 35, e2019PA003782. https://doi.org/10.1029/2019PA003782

Madsen, A.T., Murray, A.S., Andersen, T.J., Pejrup, M., 2007. Temporal changes of accretion rates on an estuarine salt marsh during the late Holocene — Reflection of local sea level changes? The Wadden Sea, Denmark. Mar. Geol. 242, 221–233. https://doi.org/10.1016/j.margeo.2007.03.001

Mai, S., Bartholomä, A., 2000. The missing mud flats of the Wadden Sea: a reconstruction of sediments and accommodation space lost in the wake of land reclamation, in: Proceedings in Marine Science. Elsevier, pp. 257–272. https://doi.org/10.1016/S1568-2692(00)80021-2

Maire, O., Lecroart, P., Meysman, F., Rosenberg, R., Duchêne, J., Grémare, A., 2008. Quantification of sediment reworking rates in bioturbation research: a review. Aquat. Biol. 2, 219–238. https://doi.org/10.3354/ab00053

Marusic, N., 2008. Waterways -- The Elbe river, life line for northern Germany, Part 2. Hansa 145, 112–115.

Mathis, M., Elizalde, A., Mikolajewicz, U., Pohlmann, T., 2015. Variability patterns of the general circulation and sea water temperature in the North Sea. Prog. Oceanogr. 135, 91–112. https://doi.org/10.1016/j.pocean.2015.04.009

McCave, I.N., Swift, S.A., 1976. A physical model for the rate of deposition of fine-grained sediments in the deep sea. Geol. Soc. Am. Bull. 87, 541. https://doi.org/10.1130/0016-7606(1976)87<541:APMFTR>2.0.CO;2

Meinshausen, M., Vogel, E., Nauels, A., Lorbacher, K., Meinshausen, N., Etheridge, D.M., Fraser, P.J., Montzka, S.A., Rayner, P.J., Trudinger, C.M., Krummel, P.B., Beyerle, U., Canadell, J.G., Daniel, J.S., Enting, I.G., Law, R.M., Lunder, C.R., O'Doherty, S., Prinn, R.G., Reimann, S., Rubino, M., Velders, G.J.M., Vollmer, M.K., Wang, R.H.J., Weiss, R., 2017. Historical greenhouse gas concentrations for climate modelling (CMIP6). Geosci. Model Dev. 10, 2057–2116. https://doi.org/10.5194/gmd-10-2057-2017

Meyenburg, G., Liebezeit, G., 1993. Mineralogy and geochemistry of a core from the Skagerrak/Kattegat boundary. Mar. Geol. 111, 337–344. https://doi.org/10.1016/0025-3227(93)90139-M

Meysman, F., Middelburg, J., Heip, C., 2006. Bioturbation: a fresh look at Darwin's last idea. Trends Ecol. Evol. 21, 688–695. https://doi.org/10.1016/j.tree.2006.08.002

Mielck, F., Hass, H.C., Michaelis, R., Sander, L., Papenmeier, S., Wiltshire, K.H., 2019. Morphological changes due to marine aggregate extraction for beach nourishment in the

German Bight (SE North Sea). Geo-Mar. Lett. 39, 47–58. https://doi.org/10.1007/s00367-018-0556-4
Mollenhauer, G., Grotheer, H., Gentz, T., Bonk, E., Hefter, J., 2021. Standard operation procedures and performance of the MICADAS radiocarbon laboratory at Alfred Wegener Institute (AWI), Germany. Nucl. Instrum. Methods Phys. Res. Sect. B Beam Interact. Mater. At. 496, 45–51. https://doi.org/10.1016/j.nimb.2021.03.016
Moros, M., Andersen, T.J., Schulz-Bull, D., Häusler, K., Bunke, D., Snowball, I., Kotilainen, A., Zillén, L., Jensen, J.B., Kabel, K., Hand, I., Leipe, T., Lougheed, B.C., Wagner, B., Arz, H.W., 2017. Towards an event stratigraphy for Baltic Sea sediments deposited since AD 1900: approaches and challenges. Boreas 46, 129–142. https://doi.org/10.1111/bor.12193
Nordberg, K., 1991. Oceanography in the Kattegat and Skagerrak Over the Past 8000 Years. Paleoceanography 6, 461–484. https://doi.org/10.1029/91PA01132
Nordberg, K., Bergsten, H., 1988. Biostratigraphic and sedimentological evidence of hydrographic changes in the Kattegat during the later part of the Holocene. Mar. Geol. 83, 135–158. https://doi.org/10.1016/0025-3227(88)90056-4
Oost, A., Colina Alonso, A., Esselink, P., Wang, Z.B., Kessel, T. van, Maren, B. van, 2021. Where mud matters: towards a mud balance for the trilateral Wadden Sea Area: mud supply, transport and deposition. Wadden Academy, Leeuwarden.
OSPAR, 2023. OSPAR Quality Status Synthesis Report 2023. oap.ospar.org.
Otto, L., Zimmerman, J.T.F., Furnes, G.K., Mork, M., Saetre, R., Becker, G., 1990. Review of the physical oceanography of the North Sea. Neth. J. Sea Res. 26, 161–238. https://doi.org/10.1016/0077-7579(90)90091-T
Paetzel, M., Schrader, H., Bjerkli, K., 1994. Do decreased trace metal concentrations in surficial skagerrak sediments over the last 15–30 years indicate decreased pollution? Environ. Pollut. 84, 213–226. https://doi.org/10.1016/0269-7491(94)90132-5
Pätsch, J., Lorkowski, I., Kühn, W., Moll, A., Serna, A., 2010. 150 years of ecosystem evolution in the North Sea-from pristine conditions to acidification. Eur. Geophys. Union Gen. Assem. 2010 Vienna Austria 2010 12291.
Peng, T.-H., Broecker, W.S., Berger, W.H., 1979. Rates of Benthic Mixing in Deep-Sea Sediment as Determined by Radioactive Tracers. Quat. Res. 11, 141–149. https://doi.org/10.1016/0033-5894(79)90074-7
Polovodova Asteman, I., Risebrobakken, B., Moros, M., Binczewska, A., Dobosz, S., Jansen, E., Sławińska, J., Bąk, M., 2018. Late Holocene palaeoproductivity changes: a multi-proxy study in the Norwegian Trench and the Skagerrak, North Sea. Boreas 47, 238–255. https://doi.org/10.1111/bor.12264
Puls, W., Heinrich, H., Mayer, B., 1997. Suspended particulate matter budget for the German Bight. Mar. Pollut. Bull. 34, 398–409. https://doi.org/10.1016/S0025-326X(96)00161-0
Pye, K., Blott, S.J., 2015. Spatial and temporal variations in soft-cliff erosion along the Holderness coast, East Riding of Yorkshire, UK. J. Coast. Conserv. 19, 785–808. https://doi.org/10.1007/s11852-015-0378-8
Qvale, G., Nigam, R., 1985. Bolivina skagerrakensis, a new name for Bolivina cf. B. robusta, with notes on its ecology and distribution. J. Foraminifer. Res. 15, 6–12. https://doi.org/10.2113/gsjfr.15.1.6
Regard, V., Prémaillon, M., Dewez, T.J.B., Carretier, S., Jeandel, C., Godderis, Y., Bonnet, S., Schott, J., Pedoja, K., Martinod, J., Viers, J., Fabre, S., 2022. Rock coast erosion: An overlooked source of sediments to the ocean. Europe as an example. Earth Planet. Sci. Lett. 579, 117356. https://doi.org/10.1016/j.epsl.2021.117356
Reimer, P.J., Brown, T.A., Reimer, R.W., 2004. Discussion: Reporting and Calibration of Post-Bomb 14C Data. Radiocarbon 46, 1299–1304. https://doi.org/10.1017/S0033822200033154

Rhoads, D.C., 1974. Organism-sediment relations on the muddy sea floor. Oceanogr. Mar. Biol. 12, 163–300.
Richter, R., 1952. Fluidal-Textur in Sediment-Gesteinen und über Sedifluktion überhaupt. Notizbl Hess Landesamtes Bodenforsch Wiesb 6: 67−81.
Rijnsdorp, A.D., Boute, P., Tiano, J., Lankheet, M., Soetaert, K., Beier, U., de Borger, E., Hintzen, N.T., Molenaar, P., Polet, H., Poos, J.J., Schram, E., Soetaert, M., van Overzee, H., van De Wolfshaar, K., van Kooten, T., 2020. The implications of a transition from tickler chain beam trawl to electric pulse trawl on the sustainability and ecosystem effects of the fishery for North Sea sole: an impact assessment. Wageningen Marine Research, IJmuiden,. https://doi.org/10.18174/519729
Robbins, J.A., 1986. A model for particle-selective transport of tracers in sediments with conveyor belt deposit feeders. J. Geophys. Res. Oceans 91, 8542–8558. https://doi.org/10.1029/JC091iC07p08542
Robbins, J.A., Edgington, D.N., 1975. Determination of recent sedimentation rates in Lake Michigan using Pb-210 and Cs-137. Geochim. Cosmochim. Acta 39, 285–304. https://doi.org/10.1016/0016-7037(75)90198-2
Rodhe, J., 1998. The Baltic and North Seas: a process-oriented review of the physical oceanography. The sea 11, 699–732.
Rodhe, J., 1996. On the dynamics of the large-scale circulation of the skagerrak. J. Sea Res. 35, 9–21. https://doi.org/10.1016/S1385-1101(96)90731-5
Rodhe, J., 1987. The large-scale circulation in the Skagerrak; interpretation of some observations. Tellus A 39A, 245–253. https://doi.org/10.1111/j.1600-0870.1987.tb00305.x
Rodhe, J., Holt, N., 1996. Observations of the transport of suspended matter into the Skagerrak along the western and northern coast of Jutland. J. Sea Res. 35, 91–98. https://doi.org/10.1016/S1385-1101(96)90738-8
Sala, E., Mayorga, J., Bradley, D., Cabral, R.B., Atwood, T.B., Auber, A., Cheung, W., Costello, C., Ferretti, F., Friedlander, A.M., Gaines, S.D., Garilao, C., Goodell, W., Halpern, B.S., Hinson, A., Kaschner, K., Kesner-Reyes, K., Leprieur, F., McGowan, J., Morgan, L.E., Mouillot, D., Palacios-Abrantes, J., Possingham, H.P., Rechberger, K.D., Worm, B., Lubchenco, J., 2021. Protecting the global ocean for biodiversity, food and climate. Nature 592, 397–402. https://doi.org/10.1038/s41586-021-03371-z
Sanchez-Cabeza, J.A., Ruiz-Fernández, A.C., 2012. 210Pb sediment radiochronology: An integrated formulation and classification of dating models. Geochim. Cosmochim. Acta 82, 183–200. https://doi.org/10.1016/j.gca.2010.12.024
Schindler, M., Karius, V., Arns, A., Deicke, M., Von Eynatten, H., 2014. Measuring sediment deposition and accretion on anthropogenic marshland – Part II: The adaptation capacity of the North Frisian Halligen to sea level rise. Estuar. Coast. Shelf Sci. 151, 246–255. https://doi.org/10.1016/j.ecss.2014.08.027
Schmidt, M., 2021. Dynamics and variability of POC burial in depocenters of the North Sea (Skagerrak), Cruise No. AL561, 2.08.2021 – 13.08.2021, Kiel – Kiel, APOC. GEOMAR Helmholtz Centre for Ocean Research Kiel. https://doi.org/10.3289/CR_AL561
Skogen, M.D., Eilola, K., Hansen, J.L.S., Meier, H.E.M., Molchanov, M.S., Ryabchenko, V.A., 2014. Eutrophication status of the North Sea, Skagerrak, Kattegat and the Baltic Sea in present and future climates: A model study. J. Mar. Syst. 132, 174–184. https://doi.org/10.1016/j.jmarsys.2014.02.004
Slavik, K., Lemmen, C., Zhang, W., Kerimoglu, O., Klingbeil, K., Wirtz, K.W., 2019. The large-scale impact of offshore wind farm structures on pelagic primary productivity in the southern North Sea. Hydrobiologia 845, 35–53. https://doi.org/10.1007/s10750-018-3653-5

Spiegel, T., Dale, A.W., Lenz, N., Schmidt, M., Sommer, S., Kalapurakkal, H.T., Przibilla, A., Lindhorst, S., Wallmann, K., 2023. Biogenic silica cycling in the Skagerrak. Front. Mar. Sci. 10. https://doi.org/10.3389/fmars.2023.1141448
Spiegel, T., Diesing, M., Dale, A.W., Lenz, N., Schmidt, M., Sommer, S., Böttner, C., Fuhr, M., Kalapurakkal, H.T., Wallmann, K., 2024a. Modelling mass accumulation rates and 210 Pb rain rates in the Skagerrak: lateral sediment transport dominates the sediment input. Front. Mar. Sci. 11. https://doi.org/10.3389/fmars.2023.1141448
Spiegel, T., Schmidt, M., Neumann, A., Moros, M., Wolschke, H., Kasten, S., Wallmann, K., 2024b. Radionuclide (210Pb, 137Cs) and mercury measurements from short sediment cores (multicorer) taken during ALKOR cruises AL557 and AL561, Skagerrak. https://doi.org/10.1594/PANGAEA.967080
Ståhl, H., Tengberg, A., Brunnegård, J., Bjørnbom, E., Forbes, T.L., Josefson, A.B., Kaberi, H.G., Hassellöv, I.M.K., Olsgard, F., Roos, P., Hall, P.O.J., 2004. Factors influencing organic carbon recycling and burial in Skagerrak sediments. J. Mar. Res. 62, 867–907. https://doi.org/10.1357/0022240042880873
Stanev, E.V., Dobrynin, M., Pleskachevsky, A., Grayek, S., Günther, H., 2009. Bed shear stress in the southern North Sea as an important driver for suspended sediment dynamics. Ocean Dyn. 59, 183–194. https://doi.org/10.1007/s10236-008-0171-4
Stevens, R.L., Bengtsson, H., Lepland, A., 1996. Textural provinces and transport interpretations with fine-grained sediments in the Skagerrak. J. Sea Res. 35, 99–110. https://doi.org/10.1016/S1385-1101(96)90739-X
Streets, D.G., Devane, M.K., Lu, Z., Bond, T.C., Sunderland, E.M., Jacob, D.J., 2011. All-Time Releases of Mercury to the Atmosphere from Human Activities. Environ. Sci. Technol. 45, 10485–10491. https://doi.org/10.1021/es202765m
Stride, A.H. (Ed.), 1982. Offshore tidal sands: processes and deposits. Chapman and Hall, London ; New York.
Syvitski, J.P.M., Vörösmarty, C.J., Kettner, A.J., Green, P., 2005. Impact of Humans on the Flux of Terrestrial Sediment to the Global Coastal Ocean. Science 308, 376–380. https://doi.org/10.1126/science.1109454
Thiede, J., 1985. Planktonic foraminifers in Upper Quaternary marine Skagerrak sediments. Nor. Geol. Tidsskr. 65, 115–118.
Thomas, H., Freund, W., Mears, C., Meckel, E., Minutolo, F., Nantke, C., Neumann, A., Seidel, M., Van Dam, B., 2022. ALKOR Scientific Cruise Report. The Ocean's Alkalinity - Connecting geological and metabolic processes and time-scales: mechanisms and magnitude of metabolic alkalinity generation in the North Sea Cruise No. AL557. Open Access. Alkor-Berichte, AL557. GEOMAR Helmholtz-Zentrum für Ozeanforschung Kiel, Kiel, Germany, 22 pp.
Toggweiler, J.R., Dixon, K., Bryan, K., 1989. Simulations of radiocarbon in a coarse-resolution world ocean model: 1. Steady state prebomb distributions. J. Geophys. Res. Oceans 94, 8217–8242. https://doi.org/10.1029/JC094iC06p08217
van Weering, T.C.E., Berger, G.W., Kalf, J., 1987. Recent sediment accumulation in the Skagerrak, Northeastern North Sea. Neth. J. Sea Res. 21, 177–189. https://doi.org/10.1016/0077-7579(87)90011-1
van Weering, T.C.E., Berger, G.W., Okkels, E., 1993. Sediment transport, resuspension and accumulation rates in the northeastern Skagerrak. Mar. Geol. 111, 269–285. https://doi.org/10.1016/0025-3227(93)90135-I
van Weering, T.C.E., Qvale, G., 1983. Recent sediments and foraminiferal distribution in the Skagerrak, northeastern North Sea. Mar. Geol. 52, 75–99. https://doi.org/10.1016/0025-3227(83)90022-1

van Wijnen, H.J., Bakker, J.P., 2001. Long-term Surface Elevation Change in Salt Marshes: a Prediction of Marsh Response to Future Sea-Level Rise. Estuar. Coast. Shelf Sci. 52, 381–390. https://doi.org/10.1006/ecss.2000.0744

Wacker, L., Fahrni, S.M., Hajdas, I., Molnar, M., Synal, H.-A., Szidat, S., Zhang, Y.L., 2013. A versatile gas interface for routine radiocarbon analysis with a gas ion source. Nucl. Instrum. Methods Phys. Res. Sect. B Beam Interact. Mater. At. 294, 315–319. https://doi.org/10.1016/j.nimb.2012.02.009

Wahl, T., Haigh, I.D., Woodworth, P.L., Albrecht, F., Dillingh, D., Jensen, J., Nicholls, R.J., Weisse, R., Wöppelmann, G., 2013. Observed mean sea level changes around the North Sea coastline from 1800 to present. Earth-Sci. Rev. 124, 51–67. https://doi.org/10.1016/j.earscirev.2013.05.003

Walling, D.E., Fang, D., 2003. Recent trends in the suspended sediment loads of the world's rivers. Glob. Planet. Change 39, 111–126. https://doi.org/10.1016/S0921-8181(03)00020-1

Wallmann, K., Diesing, M., Scholz, F., Rehder, G., Dale, A.W., Fuhr, M., Suess, E., 2022. Erosion of carbonate-bearing sedimentary rocks may close the alkalinity budget of the Baltic Sea and support atmospheric CO2 uptake in coastal seas. Front. Mar. Sci. 9, 968069. https://doi.org/10.3389/fmars.2022.968069

Wanninkhof, R., 2014. Relationship between wind speed and gas exchange over the ocean revisited. Limnol. Oceanogr. Methods 12, 351–362. https://doi.org/10.4319/lom.2014.12.351

Williams, G.P., Wolman, M.G., 1984. Downstream effects of dams on alluvial rivers (Professional Paper), Professional Paper.

Winther, N.G., Johannessen, J.A., 2006. North Sea circulation: Atlantic inflow and its destination. J. Geophys. Res. Oceans 111, 2005JC003310. https://doi.org/10.1029/2005JC003310

Tables

Table 1. Summary of sampling sites.

Station	Latitude N	Longitude E	Water depth (m)	Porosity [a]	Grain-sizes [a] D_{50} (µm)	Sediment type
MUC2	58º 10.884'	09º 47.624'	500	0.78	9	Silt, clay
MUC5	57º 45.191'	08º 17.173'	434	0.77	9	Silt, clay
MUC7	58º 18.785'	09º 34.335'	677	0.82	7	Silt, clay
MUC8	57º 59.286'	09º 14.305'	490	0.77	14	Silt, clay
MUC9	58º 04.352'	09º 05.736'	604	0.80	8	Silt, clay
St.65	58° 30.068'	09° 29.887'	530	0.79		

[a] Porosity and D_{50} (50% of particles are smaller than the given value) are means of the whole core. Detailed porosity and grain-size distributions are shown in Figure 3 and Figure 4a, b.

Table 2. Model results for the temporal variability of sedimentation rates.

Model data	MUC2 500m	MUC5 434m	MUC7 677m	MUC8 490m	MUC9 604m	St.65 530m
MAR before 1963 (g cm^{-2} yr^{-1}) [a,d]	0.22 ±0.01	0.18 ±0.01	0.11 ±0.01	0.30 ±0.02	0.12 ±0.01	0.12 ±0.01
MAR after 1963, no bioturbation (g cm^{-2} yr^{-1}) [b,d]	0.19 ±0.01	0.12 ±0.01	0.11±0.01	0.22 ±0.01	0.11 ±0.01	0.11 ±0.01
MAR after 1963, with bioturbation (g cm^{-2} yr^{-1}) [c,d]	0.10 ±0.02	0.08 ±0.02	0.08 ±0.01	0.14 ±0.03	0.06 ±0.02	0.07 ±0.01
Initial $^{210}Pb_{ex}$ activity, Pb_0 (dpm g^{-1})	32	24	44	29	29	30
Bioturbation coefficient at sediment-water interface, D_{B0} (cm^2 yr^{-1})	7.0	7.0	6.0	9.5	4.0	4.0
Attenuation coefficient for bioturbation, x_B (cm)	4.0	3.0	3.5	5.0	3.0	3.5
Porosity at sediment-water interface, ϕ_0 (-)	0.89	0.87	0.89	0.89	0.88	0.90
Porosity in compacted sediment, ϕ_c (-)	0.77	0.74	0.80	0.75	0.78	0.76
Porosity attenuation coefficient, px (cm)	0.17	0.10	0.11	0.14	0.13	0.15

[a] MAR before 1963 determined by the CFCS model below the depth of the time marker peaks (Eq. 2). [b] MAR after 1963 based on the dry sediment mass approach (Eq. 1). [c] MAR after 1963 based on reaction transport modeling including the effect of bioturbation (Eq. 3-7). [d] The uncertainty determination of the MARs is presented in detail in section 3.3.5.

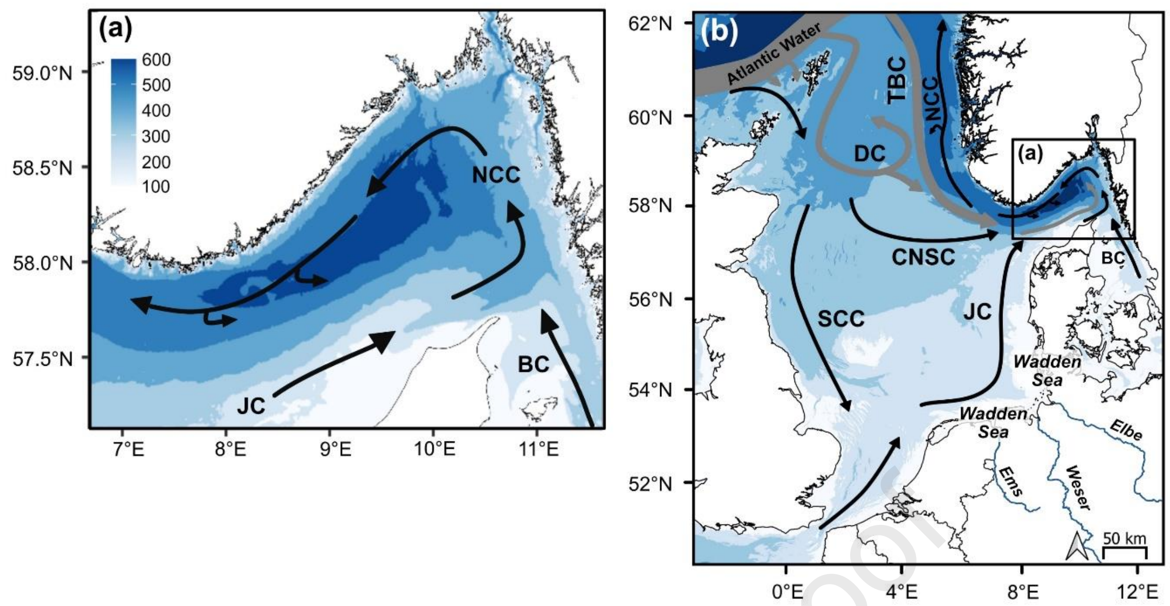

Figure 1. Study area of (a) the Skagerrak and (b) the North Sea with information on water depths, the location of the Wadden Sea and the major rivers Elbe, Weser and Ems. Black (Residual currents) and grey (Deep water currents) arrows indicate the water circulation of the Jutland Current (JC), the Baltic Current (BC), the Norwegian Coastal Current (NCC), the Tampen Bank Current (TBC), the Dooley Current (DC), the Central North Sea Current (CNSC) and the Scottish Coastal Current (SCC).

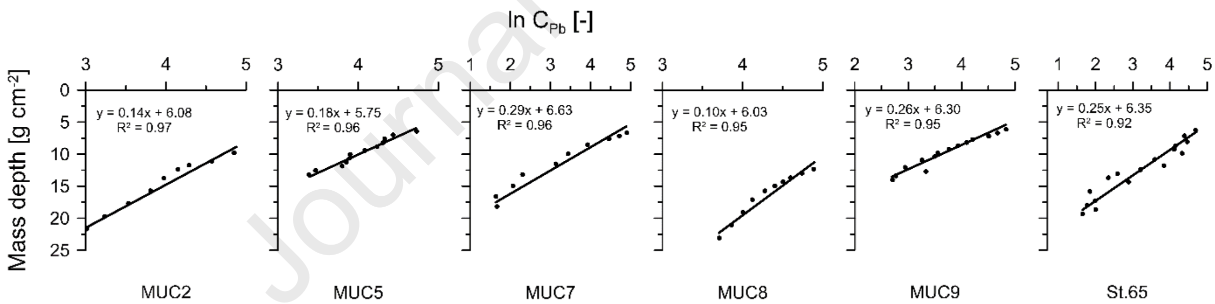

Figure 2. Modeled MARs below the depth of the time marker peaks following the CFCS method (Sanchez-Cabeza and Ruiz-Fernández, 2012) with information on the regression slope and fit. Mass depths refer to the sum of dry sediment masses above a given depth in the sediment cores.

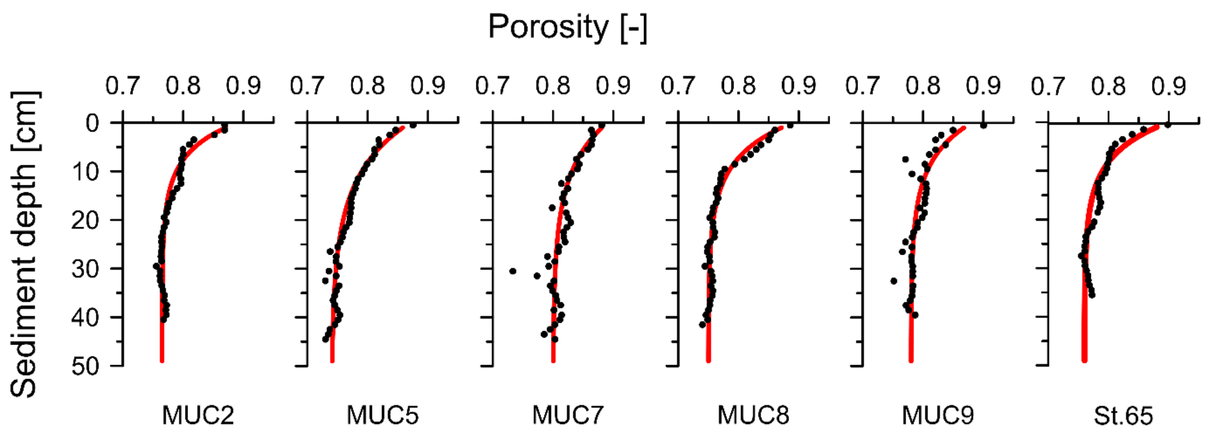

Figure 3. Measured data (symbols) and model simulations (curves) of porosity.

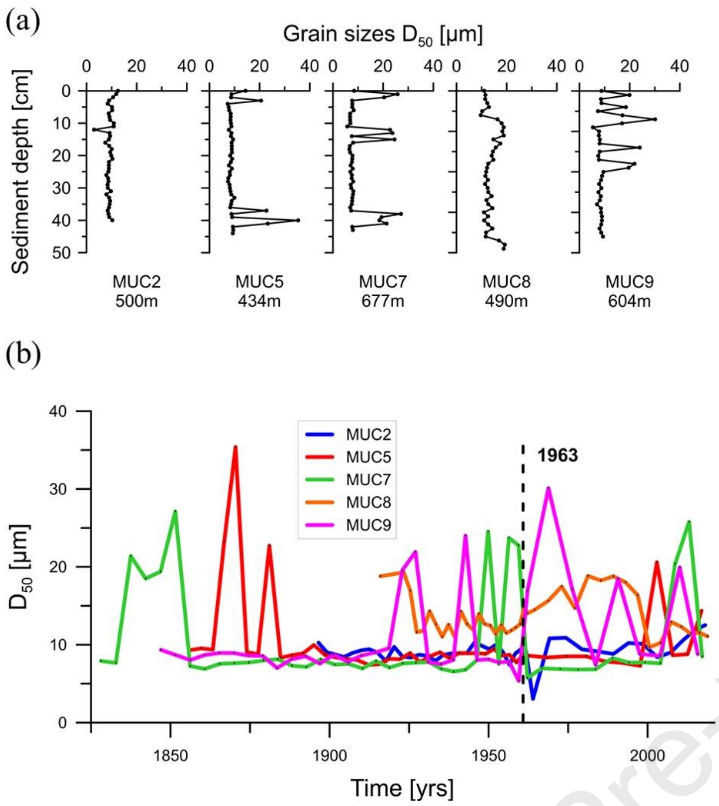

Figure 4. Median grain sizes (D_{50}) as a function of sediment depth (a) and time (b). The temporal grain size distribution is based on the MARs calculated in this study and the dashed line indicates the year 1963.

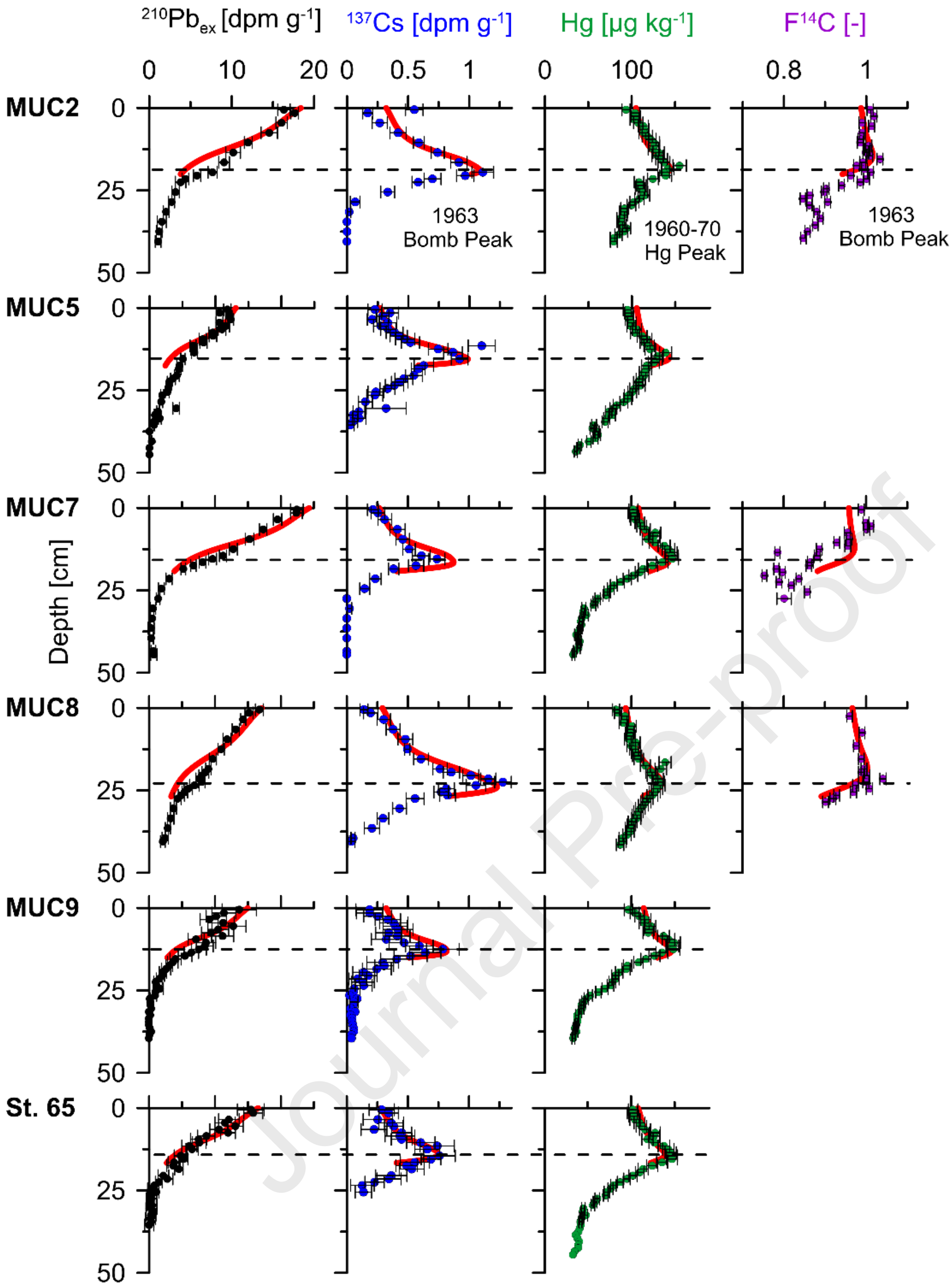

Figure 5. Measured data (symbols) and model simulations (curves) of $^{210}Pb_{ex}$ (black), ^{137}Cs (blue), Hg (green) and $F^{14}C$ (purple). The dashed lines indicate the boundary of the upper and lower sediment sections defined by the time markers of the bomb tests in 1963 and the Hg regulations in 1960 - 1970. Model simulations were conducted until slightly below the boundary depth to more accurately depict the modeled peak position.

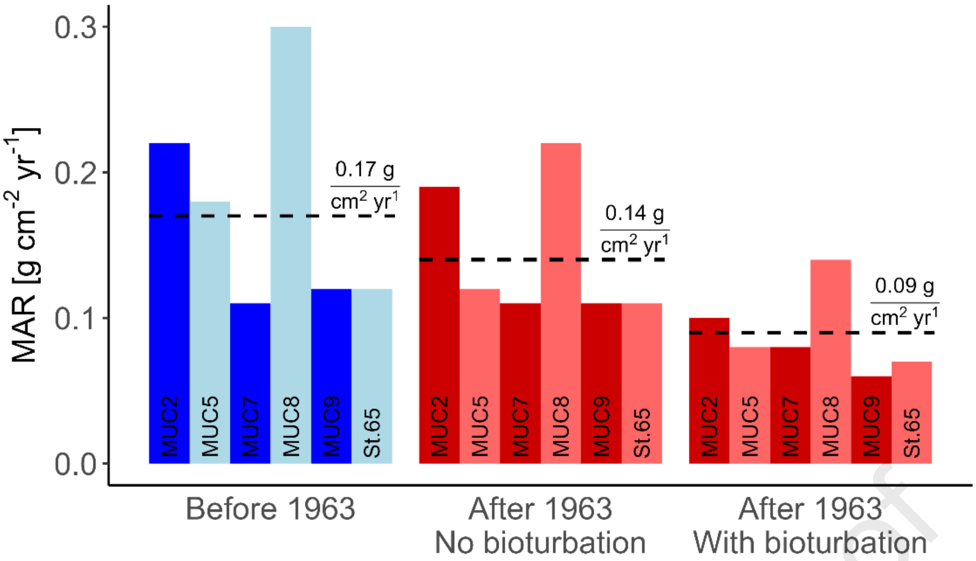

Figure 6. Modeled MARs before (blue) and after 1963 (red) at each station. The MARs after 1963 are divided into results obtained from the dry sediment mass approach (No bioturbation) and the reaction transport model (With bioturbation). The dashed lines indicate the average MAR before and after 1963.

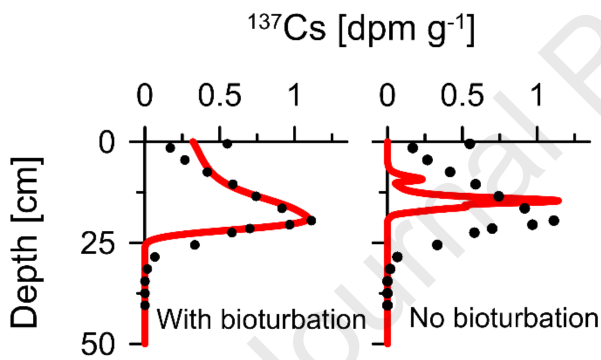

Figure 7. Measured data (symbols) and model simulations (red curves) of ^{137}Cs with the bioturbation parameters leading to the best fit (with bioturbation) and with limited bioturbation coefficients (no bioturbation). Very low coefficients (0.1 cm^2 yr^{-1}) were still necessary in the "no bioturbation" runs to maintain the numerical stability of the model.

Highlights:

- Reconstruction of mass accumulation rates in the Skagerrak
- Mass accumulation rates decreased over the last 100 years
- Decrease is more pronounced when bioturbation is considered in the reconstructions
- Findings of the Skagerrak indicate environmental shifts in the North Sea region

Declaration of interests

☒ The authors declare that they have no known competing financial interests or personal relationships that could have appeared to influence the work reported in this paper.

☐ The authors declare the following financial interests/personal relationships which may be considered as potential competing interests: